

SKB

**TECHNICAL
REPORT**

92-03

**Numerical groundwater flow
calculations at the Finnsjön study
site – extended regional area**

Björn Lindbom, Anders Boghammar

Kemakta Consultants Co, Stockholm

March 1992

SVENSK KÄRNBRÄNSLEHANTERING AB

SWEDISH NUCLEAR FUEL AND WASTE MANAGEMENT CO

BOX 5864 S-102 48 STOCKHOLM

TEL 08-665 28 00 TELEX 13108 SKB S

TELEFAX 08-661 57 19

NUMERICAL GROUNDWATER FLOW CALCULATIONS AT THE
FINNSJÖN STUDY SITE - EXTENDED REGIONAL AREA

Björn Lindbom, Anders Boghammar

Kemakta Consultants Co, Stockholm

March 1992

This report concerns a study which was conducted for SKB. The conclusions and viewpoints presented in the report are those of the author(s) and do not necessarily coincide with those of the client.

Information on SKB technical reports from 1977-1978 (TR 121), 1979 (TR 79-28), 1980 (TR 80-26), 1981 (TR 81-17), 1982 (TR 82-28), 1983 (TR 83-77), 1984 (TR 85-01), 1985 (TR 85-20), 1986 (TR 86-31), 1987 (TR 87-33), 1988 (TR 88-32), 1989 (TR 89-40) and 1990 (TR 90-46) is available through SKB.

**Numerical groundwater flow calculations
at the Finnsjön study site –
extended regional area**

by

**Björn Lindbom
Anders Boghammar**

**Kemakta Consultants Co.
Pipersgatan 27
112 28 Stockholm, Sweden**

Abstract

The present report describes modelling efforts of the groundwater flow situation at the Finnsjön site in northern Uppland, approximately 140 km north of Stockholm. The study forms part of the SKB 91 performance assessment project, and aims at describing the travel times and travel paths from a potential repository for spent nuclear fuel located in crystalline rock, and also to calculate the flux values at repository level. The groundwater flow equations were solved with the finite element technique and made use of the NAMMU-code for stationary calculations in three dimensions.

The calculations aimed at identifying a reference case from which the boundary pressures were to be extracted and used as input for future calculations with the HYDRASTAR-code, which is based on the stochastic continuum approach. The study also comprises an analysis to investigate the model sensitivity to the conductivity contrast between rock mass and fracture zones, the sensitivity to the presence of sub-horizontal fracture zones, and the degree of establishment of the discharge area.

The fracture zones were modelled implicitly with an averaging technique.

Stockholm, March, 1992.

Summary

The present project forms part of the SKB 91 performance assessment project. It is devoted to numerical groundwater flow calculations at the Finnsjön study site and forms part of a series of studies aiming at the description of the groundwater flow situation at the site.

Prior to this study, an initial study was conducted which involved the modelling of a regional scale area. The present study covered a larger area than that in the previous study, and furthermore, the fracture zones within the modelled area were modelled implicitly with an averaging technique developed by Kemakta. The extended area incorporated the modelling of three more zones, that were located outside the previously modelled area.

The eight cases that were included in the study, were based on an upscaling procedure of the hydraulic conductivities derived from the field investigations (packed-off bore hole sections with 2-3 m length) and made use of an averaging length of 36 m. The main purpose for the present project has been to create a reference case and to transfer pressure boundary conditions from the calculation cases as being input to future calculations with the HYDRASTAR-code, a code which is based on a stochastic continuum approach. Furthermore, the intention has been to investigate the sensitivity of the model results with regard to different assumptions concerning contrast in hydraulic conductivity between the rock mass and the fracture zones, the establishment of the discharge area, and the sensitivity to the presence of sub-horizontal highly permeable fracture zones.

The Base Case involved the modelling of the rock mass and fracture zones with a maximum conductivity contrast of a factor of about 35 between the rock mass and the highly permeable zone 2. The contrasts between the rock mass and the remaining fracture zones were about 10-20. The fluxes at repository level amounted to about $0.001 \text{ m}^3/\text{m}^2/\text{year}$ as a median value, while the upper quartile value was almost about $0.002 \text{ m}^3/\text{m}^2/\text{year}$. The travel times for water particles from the repository were about 450 years (a flow porosity of 0.0001) with average path lengths of about 5500 m. The point of discharge was located just by the model boundary in the northern part of the modelled domain in the Imundbo zone.

Two cases addressing the sensitivity to conductivity contrasts (increased to a factor of about 400), showed that the model is very sensitive to an increased fracture zone conductivity, resulting in a 70% reduction of travel times as an average. The fluxes at repository level were increased with roughly one order of magnitude at most. The situation with an increased contrast by a reduced rock mass conductivity showed that the travel times are twice as high as for the Base Case. This depends of course on the increased residence time in the rock. The fluxes at repository level were reduced accordingly, one order of magnitude at most.

Three cases were concerned with the sensitivity to the presence of major sub-horizontal permeable fracture zones. These indicated a strong influence particularly for the situation with a generic zone (assumed undetected hitherto) below the repository without the presence of a similar zone above the repository; the latter acts a separator for vertical flow exchange between the regions above and below the zone, respectively. This case showed travel times that were reduced with about 85% compared to the Base Case, depending on a vertical downward transport from the repository to the sub-horizontal zone and a further transport in this zone to the model boundary. The two cases with the generic zone modelled showed median flux values being roughly twice as high as the other cases (about $0.002 \text{ m}^3/\text{m}^2/\text{year}$) and upper quartile values of about $0.003\text{-}0.006 \text{ m}^3/\text{m}^2/\text{year}$.

The discharge point for released water particles was rather well defined by the model for all cases studied; the major discharge collector was the Imundbo zone. The confidence in this statement was tested by treating the Imundbo zone as rock mass and by changing the dip of the Imundbo zone from vertical to 45° SW (towards the repository) in order to analyse the effects of an increased gradient at greater depths. Both cases reinforced the impression that the area in the vicinity of the Imundbo zone was the major discharge area. When the Imundbo zone was assigned rock mass

conductivity the flow paths reached the ground surface closer to the repository. The travel times were, however, not affected significantly. The situation with the zone sloping indicated longer travel times (roughly 900 years as an average) than for the Base Case, mainly depending on a transfer of the surficial topography to greater depths which implied a drainage to the Imundbo zone at depth, which in turn increased the residence time in the rock mass.

As a result of the averaging technique when assigning fracture zone properties, it was concluded that peak values, that usually are obtained with specific fracture zone elements, were less pronounced. This conclusion goes for both travel times and flux values, and the consequences naturally depend on that the fracture zone properties are averaged over a larger volume of the domain than with ordinary "specific fracture zone element technique".

The knowledge of the hydraulic properties of some of the fracture zones within the site is limited. The results indicated that the model was sensitive to a substantially increased fracture zone conductivity.

Perhaps the most serious source of uncertainty, is the situation when a fracture zone remains undetected despite an extensive field investigation (corresponding to the case with a generic zone modelled); particularly if the zone is permeable and extends over large areas. This situation was found to be the most sensitive one that was studied within this project, since it affected not only the travel times from the repository but also the fluxes at repository level. The latter may in turn affect the efficiency of the engineered barriers in the proximity of the repository, and the presence of the permeable fracture zone provides means for a fast transport of the potentially dissolved radionuclides from the repository.

Table of Contents

	Page
1. Introduction	1
1.1 Purpose and Scope of the Project	1
1.2 Brief Description of NAMMU	3
2. Case Descriptions – Boundary Conditions – Hydraulic Properties	4
3. Modelling Results	14
3.1 The Base Case (Case X36)	14
3.2 Parameter Variations	19
3.2.1 Sensitivity to Contrasts in Hydraulic Conductivity (Cases X36FR and X36RM)	19
3.2.2 Sensitivity to Major Permeable Sub-Horizontal Fracture Zones (Cases X36V1, X36V3 and X36V4)	23
3.2.3 Confidence in the Location of the Discharge Area – Imundbo (Cases X36V2 and X36IM)	27
4. Summary and Conclusions	31
References	33
List of Symbols	34
Appendix A Documentation of files created and processed during the project	
Appendix B Evaluation figures not presented in the current text	

1. Introduction

1.1 Purpose and Scope of the Project

The present project forms part of the SKB 91 performance assessment project. It is devoted to numerical groundwater flow calculations at the Finnsjön study site and forms part of a series of studies aiming at the description of the groundwater flow situation at the site.

Prior to the present project, some initial calculations were performed. These indicated that the major discharge area was located in the vicinity of the regional lineament Imundbo, see Figure 1.1. The flow was driven to this area mainly by the regional NE gradient, and was discharged in the Imundbo zone by a local NW directed gradient. The travel times from the potential repository to the model boundary were found to be in the range of 500-2500 years assuming a flow porosity of 10^{-4} . Due to the groundwater topography and the interaction between some local fracture zones (zones 1, 2, 3 and 4), the particles were collected in an area where these local zones intersected. From this point they were all transported to the Imundbo lineament. Typical flux values at repository level were about $0.0001 \text{ m}^3/\text{m}^2/\text{year}$. The results from these calculations are reported in (KEM1, 1991).

The main purpose for the present project has been to create a reference case for the far field flow analysis within the SKB 91 programme. Furthermore, the intention has been to investigate the sensitivity of the model results with regard to different assumptions concerning the hydraulic conductivity contrast between the rock mass and the fracture zones, the sensitivity to the presence of major sub-horizontal fracture zones, and the degree of uncertainty in the location of the discharge area.

Of particular concern was to generate pressure boundary conditions for future calculations with the HYDRASTAR-code, a code which is based on the stochastic continuum approach. The input scheme to HYDRASTAR generates hydraulic conductivity values based on different averaging lengths of bore hole data. The hydraulic conductivity distribution that has been evaluated from the input scheme of the HYDRASTAR-code is based on an averaging length of 36 m, a length to which bore hole data from packed-off sections with a length of 2-3 m have been upscaled. This upscaling procedure is based on single-hole injection tests.

The origin of the background data is (SGAB1, 1991), while the data as interpreted for modelling purposes can be found in (KEM1, 1991). The areal coverage (about 40 km^2) of the regional scale model in the KEM1-study was smaller than that considered in the present project. The areal coverage of the studied domain in the present study is roughly 80 km^2 . The extended area incorporated the modelling of three more zones, that were located outside the previously modelled area, see Figure 1.1. All fracture zones were modelled implicitly with an averaging technique developed by Kemakta in the IFZ-code (KEM1, 1991) in the present study.

The calculations have been performed in three dimensions and made use of the NAMMU-package (HARW1, 1979 and HARW2, 1985) for solving the flow equation using the finite element technique, while the HYPAC-package (KEM2, 1989) was used for pre- and postprocessing purposes. One of the codes within the HYPAC-package, called TBCSTA, was specially designed for extracting the boundary pressures along the confinements of the model, and to write them in a format adapted for direct application to the input routines in HYDRASTAR.

The coordinate system used is the RAK-system with an offset in $y=1600000 \text{ m}$ and $x=660000 \text{ m}$, the same offset as was used in (SGAB1, 1991).

1.2 Brief Description of NAMMU

The flow system at the site is solved numerically with the computer code NAMMU (HARW1, 1979, HARW2, 1985), which is a computer code developed to simulate coupled heat and groundwater flow in either one, two or three dimensions. It is a finite-element model with the continuum approach based on the flow equation (flow through porous media). The two dependent variables to be determined in NAMMU are the non-hydrostatic pressure and the temperature. The two coupled partial differential equations being solved for stationary conditions are:

$$\frac{\partial}{\partial t} (\epsilon \rho^f) + \nabla \cdot (\rho^f \bar{q}) = 0 ,$$

and

$$(\rho c_p)_s \frac{\partial T}{\partial t} + \rho^f c_p^f \bar{q} \cdot \nabla T - \Gamma_s \nabla^2 T = H ,$$

where $(\rho c_p)_s$ is given by

$$(\rho c_p)_s = \epsilon \rho^f c_p^f + (1 - \epsilon) \rho^s c_p^s .$$

The Darcy velocity \bar{q} is given by

$$\bar{q} = - \frac{k}{\eta} (\nabla p_d - (\rho^f - \rho^s) \bar{g}) .$$

A list of the symbols used is given at the end of the report.

The equations are discretised in space using the Galerkin finite-element method, discretised in time by backward finite-difference schemes with time-stepping using Gear's method. The resulting non-linear algebraic equations are generally linearised by the Newton-Raphson method and then solved by a direct frontal solver. The present study utilises only a subset of NAMMU dealing with steady-state groundwater flow in a saturated medium. In this case, the equations generated are linear and no time-stepping is required.

NAMMU is implemented on a Convex, model C-220. The calculations performed within this project were carried out in three dimensions with 8-noded brick elements, which means that the interpolation between element corners is linear. NAMMU version 4S has been used within the present project.

The particle tracking as presented in the report is based on a Euler technique, i.e. with a simple forward stepping. The step-length is specified by the user; the tracking routine forms part of the HYPAC program package, (KEM2, 1989).

The entity "flux" as reported in the study, equal to the "Darcy velocity" or the "volumetric flux", is expressed in $\text{m}^3/\text{m}^2/\text{year}$, and is calculated according to the formula:

$$|\bar{q}| = \sqrt{q_x^2 + q_y^2 + q_z^2} .$$

See the "List of Symbols" for an explanation of the symbols used.

2. Case Descriptions – Boundary Conditions – Hydraulic Properties

The hydraulic conductivity distribution for all cases within the study, was based on an upscaling procedure (a so called regularisation) of packed-off borehole sections with a length of 2-3 m, to an averaging length of 36 m. The conductivities assigned to the rock mass and the fracture zones within the present study, were obtained from part of the input scheme to the HYDRASTAR-code.

Of primary concern for the project has been to create a reference case, from now on called Case X36, and to have the boundary pressures transferred from these calculations to future calculations with the HYDRASTAR-code. Apart from the calculation of Case X36, the project has been focussed on three main sources of uncertainty aiming at elucidating the sensitivity to different assumptions with regard to the conductivity contrast between the rock mass and the fracture zones, the presence of major permeable sub-horizontal fracture zones, and to the degree of confidence in the discharge area. To this end, seven calculation cases have been performed in addition to the Base Case. All statements below like "increased", "reduced", etc, refer to comparisons with Case X36. The main features and aims are given below:

The Base Case

Case X36: By the upscaling procedure mentioned above, new conductivity data, compared to the values used in the KEM1-study, for the rock mass and for zone 2. The remaining fracture zones were assigned hydraulic conductivities so that the contrasts in conductivity between individual fracture zones and the rock mass were scaled according to interpretations made by geologists. The regularisation procedure implied that the conductivity contrast between the rock mass and the fracture zones is significantly lower than was the situation in the KEM1-study.

Sensitivity to different conductivity contrasts

Since the contrasts in hydraulic conductivity between the rock mass and the fracture zones in Case X36 were much smaller than for the cases considered in the KEM1-study, questions arose as to how much this possible source of uncertainty might affect the results; or in other words to see if there is a limit to when the flow is fracture dominated or matrix dominated. Two cases were studied:

Case X36FR: A contrast of roughly three orders of magnitude (instead of about 1.5 orders of magnitude as in Case X36) between the rock mass and all fracture zones, except for zone 2, has been assumed for this case by increasing the fracture zone conductivity. The main purpose was to investigate the model sensitivity to the increased fracture zone conductivity in terms of travel times from the repository, i.e. to what degree the water particles are transported in the fracture zones in this situation.

Case X36RM: A contrast of roughly three orders of magnitude (instead of about 1.5 orders of magnitude as in Case X36) between the rock mass and the fracture zones has been assumed for this case by reducing the rock mass conductivity. The main purpose was also here to investigate the model sensitivity to the reduced rock mass conductivity in terms of travel times from the repository.

Sensitivity to the presence of major sub-horizontal fracture zones

Previous studies have shown that the major sub-horizontal permeable fracture zone 2 at the site, is vital for the overall flow system, since it effectively separates the flow vertically into two regimes, one flow domain above the zone with relatively high fluxes and one below the zone with lower fluxes. This implies that zone 2 reduces the fluxes at repository level. Furthermore, it has in other studies (KEM3, 1989) been shown that the presence of a similar zone located below the repository could increase the fluxes at repository level substantially, and provide excellent pathways for

released radionuclides. Three set-ups have therefore been considered in order to investigate the model sensitivity to the presence of zone 2 and to the presence of a generic zone located below the repository with properties similar to those of zone 2:

Case X36V1: The model sensitivity to the presence of the major sub-horizontal fracture zone 2 was investigated by treating the zone as being part of the rock mass.

Case X36V3: A situation with a generic sub-horizontal zone called zone 2u (located below zone 2 and the repository) was analysed. The zone was assumed to have the same properties as zone 2, and to be parallel to zone 2. The vertical distance between the mid-points of the two zones was assumed to be 600 m. The inclination of zone 2u was assumed to be the same as that of zone 2. The two zones differ in their areal coverage so that zone 2 is assumed to be confined by zones 1, 4 and 12, whereas zone 2u is assumed to extend to the confinements of the modelled domain.

Case X36V4: This case is concerned with the importance of zone 2u without the presence of zone 2. This implies that zone 2 in this case is treated as rock mass, while zone 2u is modelled in accordance with Case X36V3.

Confidence in the location of the discharge area

The KEM1-study indicated that the Imundbo zone acted as the major discharge area for particles released within the potential repository. Since the zone has not been penetrated by any boreholes, its properties are uncertain and based on similarities with the local fracture zone 5 within the local scale block, see (SGAB1, 1991). Furthermore, there is no evidence for the zone being vertical. This lack of information is a source of uncertainty and the effect of it is investigated accordingly:

Case X36V2: The draining capacity of the area around the Imundbo zone, and the importance of the zone in this context, was investigated by treating the Imundbo zone as rock mass, and hereby analysing whether the topography of the area around the zone was pronounced enough to act as a discharge area without the Imundbo zone.

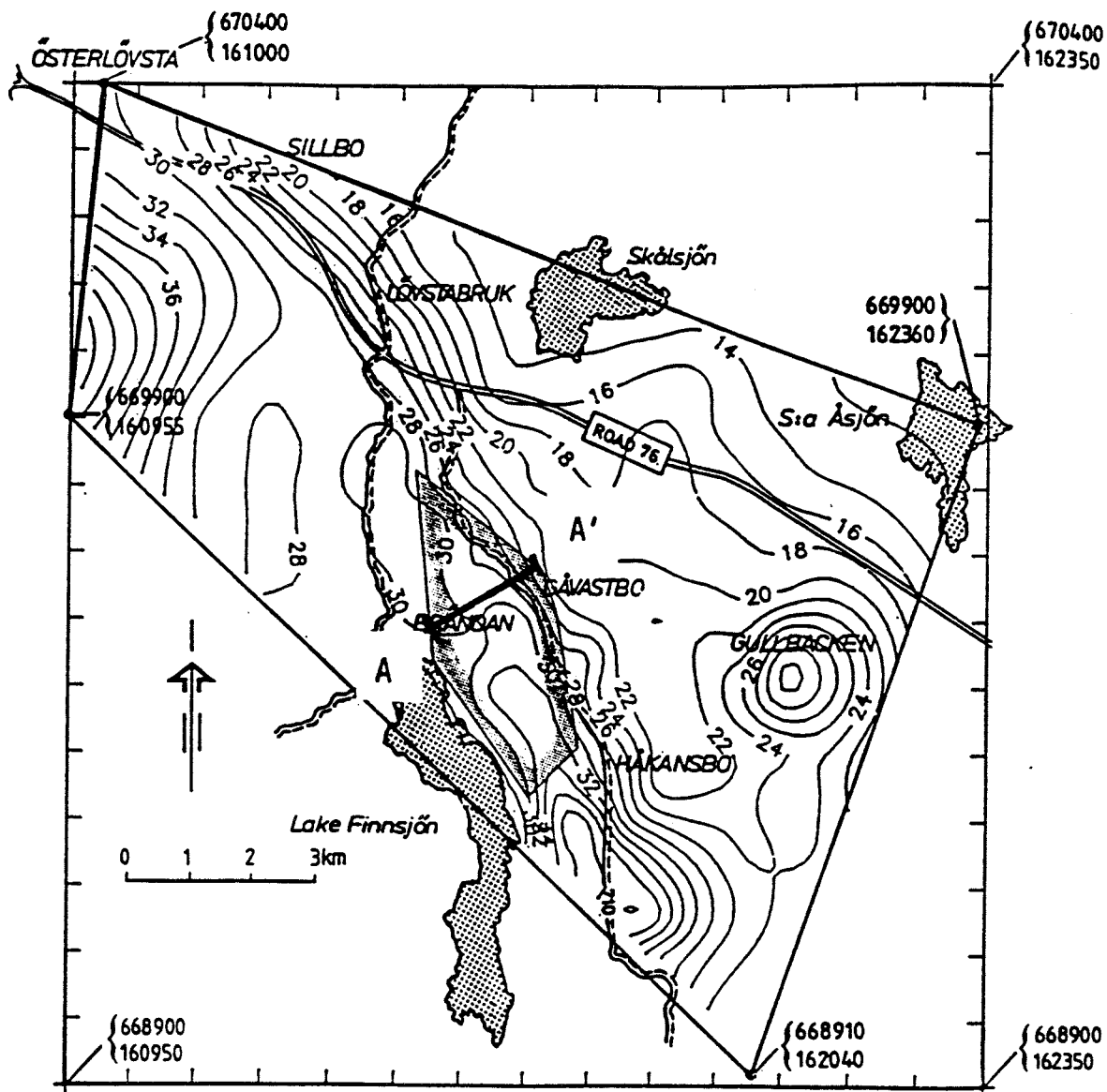
Case X36IM: The sensitivity to an inclination other than vertical was investigated by changing the dip of the Imundbo zone to 45° SW, i.e. in a manner so that it comes closer to the repository area with increasing depth.

The lateral and bottom boundaries were of no-flow type for all the cases, whereas the upper boundary condition was of a prescribed "zero-pressure" type; i.e. the natural groundwater topography as shown in Figure 2.1. forms the upper boundary.

The sub-horizontal zone 2 is known to be of great importance for the flow system at the site, and has been subjected to extensive field investigations. It is confined by zones 1, 4, 12 and 7 (see Figures 1.1 and 2.2). The latter is a minor fracture zone present on the local scale and not considered within the present study. Its strike is WE and it intersects with zones 1 and 12 at about two thirds of the distance between zone 4 and zone 14. Zone 2 reaches the ground surface partly at its intersection with zone 4. For a detailed description of zone 2, see (SGAB1, 1991).

Since both zone 2 and zone 2u are inclined, their distances to the repository vary. The shortest distance from the repository to zone 2 is about 230 m (SE corner of the repository), and for zone 2u the corresponding distance is about 100 m (NW corner of the repository). Figure 2.3 shows the logarithmic conductivity distribution in a vertical cross-section (SW-NE) through the repository area aiming at illustrating the two sub-horizontal zones.

The shortest distance from the repository to the Imundbo zone is about 1750 m for all cases, except for Case X36IM, where the distance was reduced to 800 m due to the inclination of the Imundbo zone.



LEGEND:

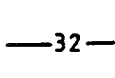
- Road 
- Minor road 
- Groundwater table contour 

Figure 2.1 Topography of the semi-regional as considered within the present project (from SGAB1, 1991). Cross-section A-A' corresponds to Figure 2.2.

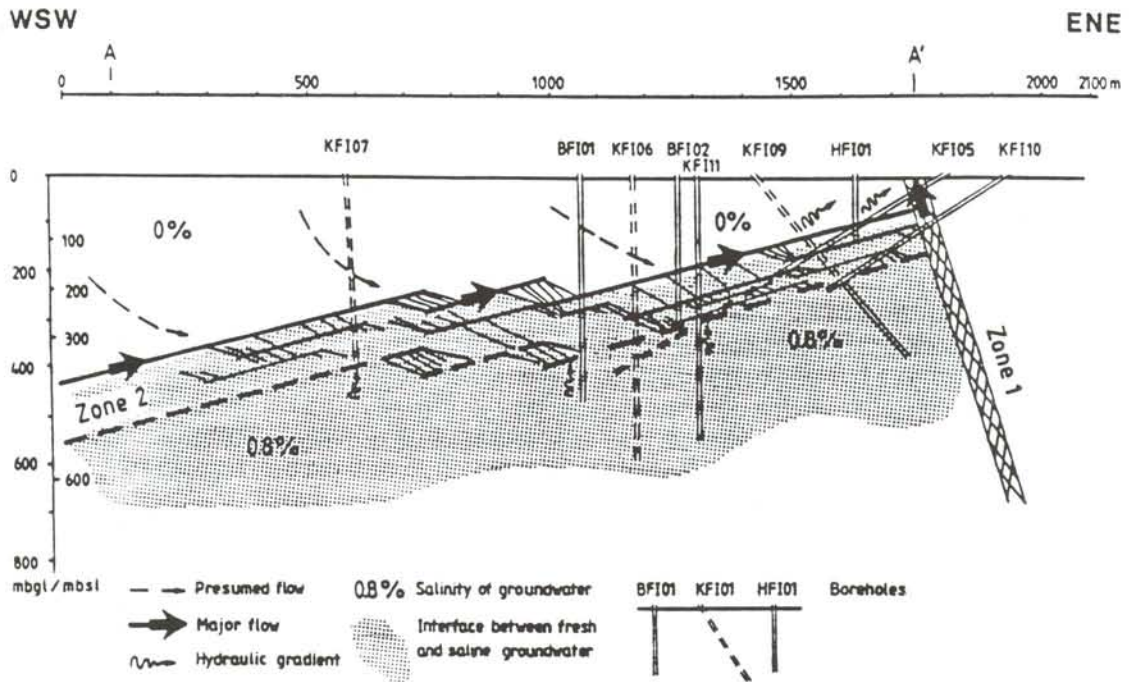


Figure 2.2 Tentative conceptual model for the groundwater flow in zone 2 (SGAB1, 1991). See Figure 2.1 for the location of cross-section A-A'.

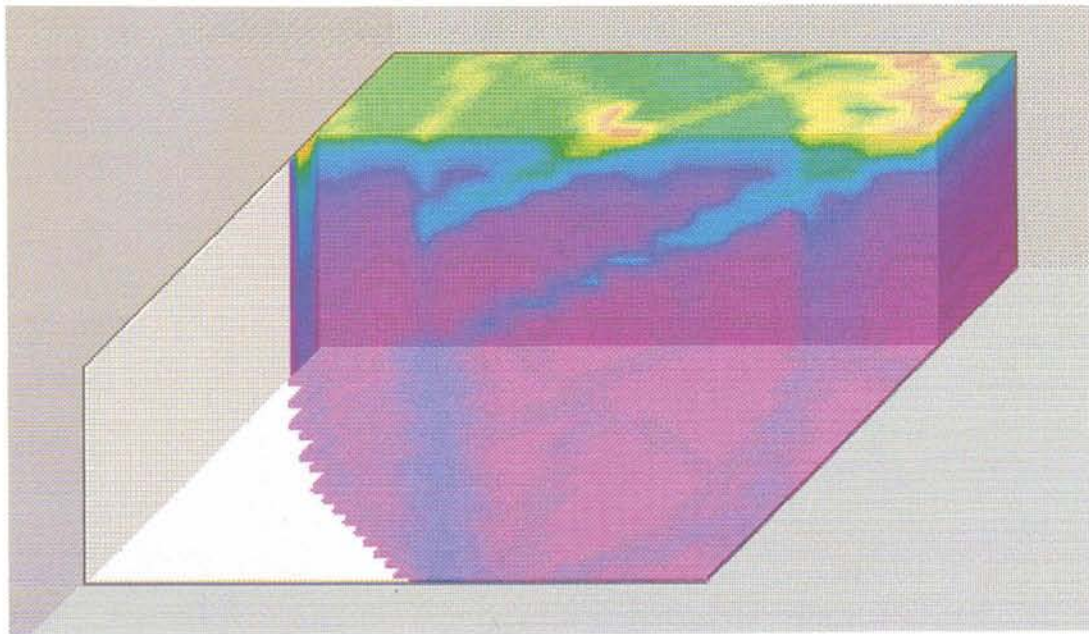


Figure 2.3 Logarithmic conductivity distribution for a sub-set of the modelled domain. The cross-section cuts through the repository area and illustrates the two sub-horizontal zones 2 and 2u; the latter being generically modelled for Cases X36V3 and X36V4. The depth of the domain as plotted is 1000 m. The conductivity decreases with increasing darkness of the colours. The two zones are visible as two parallel light blue bands in the upper part of the domain.

The increased areal extension of the model has incorporated a few fracture zones that were not included in the KEM1-study. These fracture zones are from now on referred to as zones Giboda S, NS1 and NS2, see Figure 1.1 for their locations. Their hydraulic properties were judged according to their nearness and similarities to the Giboda zone and zone 4 for zone Giboda S, and the similarity between zone 12 and zones NS1 and NS2 (SGAB2, 1991). The fracture zone geometries are shown in Table 2.1. All fracture-zone conductivities were assigned implicitly with the IFZ-code. Furthermore, the calculations of Cases X36V3 and X36V4 have incorporated a generic sub-horizontal zone (zone 2u), reaching the ground surface at the approximate position as indicated in Figure 1.1 and dipping SW according to Table 2.1.

The depth dependence of the rock mass conductivity and the fracture zone conductivities is shown graphically in Figure 2.4a for Case X36, in Figure 2.4b for Case X36FR, and in Figure 2.4c for Case X36RM. (For comparison, corresponding values that were used within the KEM1-study are shown in Figure 2.4d.) The distribution of the logarithmic hydraulic conductivities for Case X36 in a subset of the area is shown in three colour plots in Figures 2.5a-c at depths of $z=0$, $z=-300$ m, and $z=-600$ m, respectively. The plots illustrate rather clearly the locations of the fracture zones, and indicate the order of magnitude of the hydraulic conductivities and their distribution with depth. The dark blue areas indicate regions with low conductivity. The conductivity increases with decreasing darkness of the colours.

Table 2.1 Fracture zones in the Finnsjön area as modelled within the present project. For further information with regard to background values, see (SGAB1, 1991). The abbreviations for the regional lineaments in the table refer to their notations in Figures 2.4a-d.

Zone	Width (m)	Inclination (degrees)
1	20	75 SE
2	100	16 SW
2u ¹	100	16 SW
3	50	80 SW
4	10	60 SW
12	50	90
13	50	90
14	50	90
Skogsbo (Sk)	100	90
Giboda (Gi)	100	90
Imundbo (Im) ²	100	90
Gräsbo (Gr)	100	90
Dannemora (Da)	100	90
Källviken (Kä)	100	90
Giboda S ³ (GiS)	50	90
NS1 (NS1)	50	90
NS2 ⁴ (NS2)	25	90

¹ The zone is generic and is assumed to have the same properties as zone 2, but located at a vertical distance of 600 m below zone 2. The zone is modelled only for Case X36V3 and Case X36V4.

² The zone is inclined 45° SW for Case X36IM.

³ The zone is assumed to have the same hydraulic properties as the Giboda zone, but with an intermediate width between zone 4 and the Giboda zone.

⁴ The zone is assumed to have the same hydraulic properties as zone 12, but with a different width.

The geometries of the fracture zones are identical for all cases, except for Case X36IM (see footnote to Table 2.1). The conductivities for the fracture zones were assigned according to Table 2.2. The conductivities for both the rock mass and the fracture zones were assumed to obey the formula $K=a \cdot z^{-b}$. The value of the factor "a" is given for each fracture zone in Table 2.2. All fracture zones and the rock mass are assumed to have the same depth dependence with the exponent "b" equal to 2.23. Not being present in Table 2.2, note that the hydraulic properties of Cases X36RM and X36IM are equal to those of Case X36, except that the value of the factor "a" is equal to 0.0121 for the rock mass for all the cases except for Case X36RM where the factor "a" has the value 0.00121, and that Case X36IM differs in that the Imundbo zone inclines according to Table 2.1.

Table 2.2 *Hydraulic conductivities on the form $K=a \cdot z^{-b}$ of the fracture zones as modelled within the present project. The value of the factor "b" is equal to 2.23 for all fracture zones and the rock mass. The notation "RM" means rock mass. The abbreviations for the regional lineaments in the table refer to their notations in Figures 2.4a-d.*

Case : → Zone : ↓	X36 a ↓	X36FR a ↓	X36V1 a ↓	X36V2 a ↓	X36V3 a ↓	X36V4 a ↓
1	0.187	2.44	0.187	0.187	0.187	0.187
2	0.427	0.427	RM	0.427	0.427	RM
2u ¹	RM	RM	RM	RM	0.427	0.427
3	0.140	1.40	0.140	0.140	0.140	0.140
4	0.118	1.00	0.118	0.118	0.118	0.118
12 ²	0.118	1.00	0.118	0.118	0.118	0.118
13 ³	0.187	2.44	0.187	0.187	0.187	0.187
14 ²	0.118	1.00	0.118	0.118	0.118	0.118
Skogsbo (Sk) ⁴	0.270	4.99	0.270	0.270	0.270	0.270
Giboda (Gi) ⁴	0.270	4.99	0.270	0.270	0.270	0.270
Imundbo (Im) ⁴	0.270	4.99	0.270	RM	0.270	0.270
Gräsbo (Gr) ²	0.118	1.00	0.118	0.118	0.118	0.118
Dannemora (Da) ²	0.118	1.00	0.118	0.118	0.118	0.118
Källviken (Kä) ³	0.187	2.44	0.187	0.187	0.187	0.187
Giboda S ⁵ (GiS)	0.270	4.99	0.270	0.270	0.270	0.270
NS1 ⁶ (NS1)	0.118	1.00	0.118	0.118	0.118	0.118
NS2 ⁷ (NS2)	0.118	1.00	0.118	0.118	0.118	0.118

¹ The zone is generic and assumed to have the same properties as zone 2, but located at a vertical distance of 600 m below zone 2. The zone is modelled only for Case X36V3 and Case X36V4.

² Hydraulic properties assumed to be similar to those of the Singö-fault, see (SGAB1, 1991).

³ Hydraulic properties assumed to be similar to those of zone 1.

⁴ Hydraulic properties assumed to be similar to those of local fracture zone 5, see (SGAB1, 1991).

⁵ The zone is assumed to have the same hydraulic properties as the Giboda zone, but with an intermediate width between zone 4 and the Giboda zone.

⁶ The zone is assumed to have the same hydraulic properties as zone 12.

⁷ The zone is assumed to have the same hydraulic properties as zone 12, but with a different width.

A top view of the finite element mesh that was generated is shown in Figure 2.6. The mesh contains about 18400 eight-noded brick elements, with a total of about 20700 nodes for all cases except for Cases X36V3 and X36V4. The mesh was conditioned so that the mesh density was increased, to highest possible degree, to coincide with the strike of the fracture zones and the regional flow pattern. The same mesh has been used for all cases, except for Case X36V3 and Case X36V4, which needed a vertical refinement of the mesh in order to appropriately account for the additional sub-horizontal zone (zone 2u) that was modelled for these cases. The meshes for the latter two cases consisted of about 25700 elements with a total of about 28500 nodes.

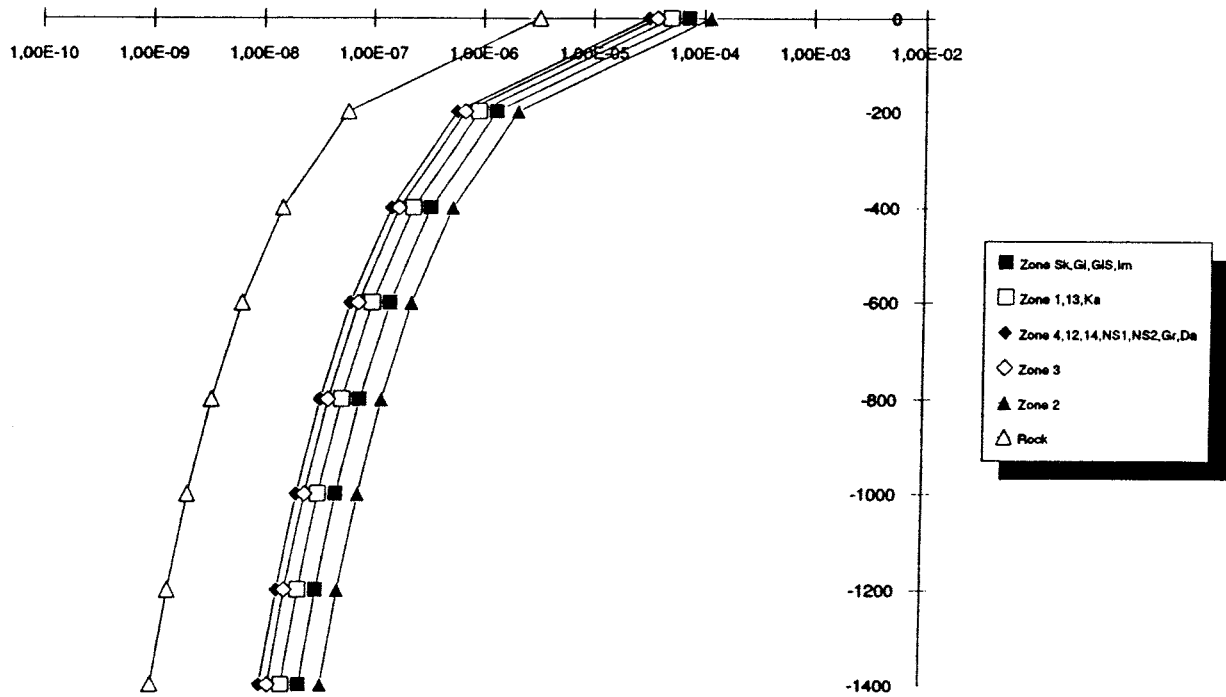


Figure 2.4a Depth dependence of rock mass conductivity and fracture zone conductivities for Case X36.

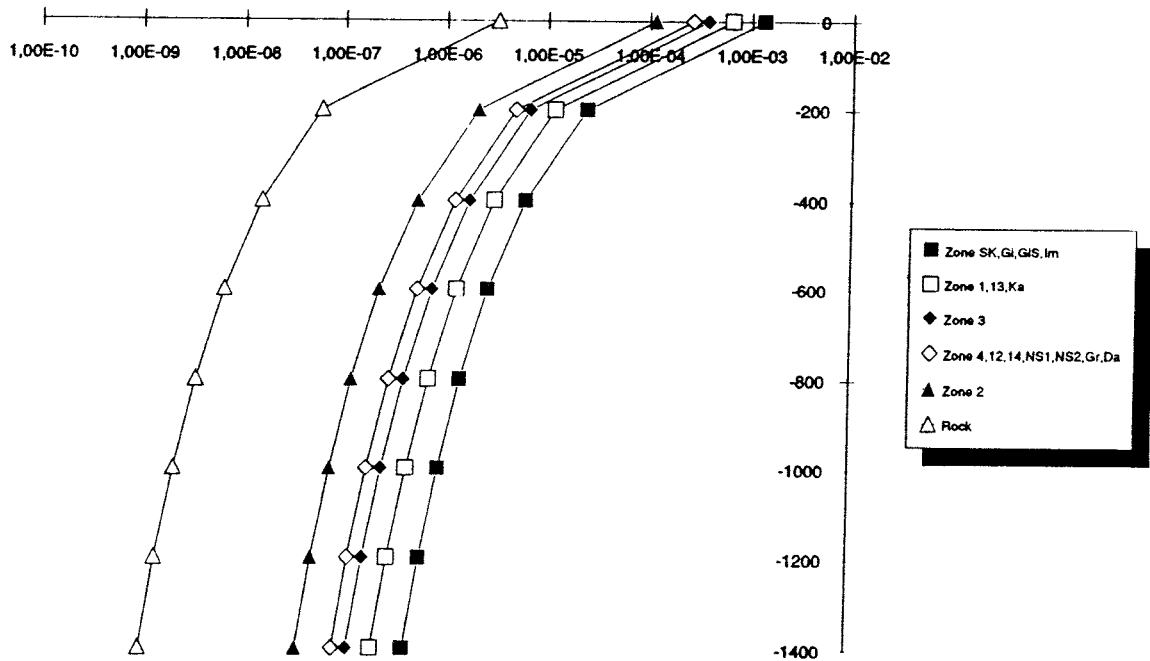


Figure 2.4b Depth dependence of rock mass conductivity and fracture zone conductivities for Case X36FR.

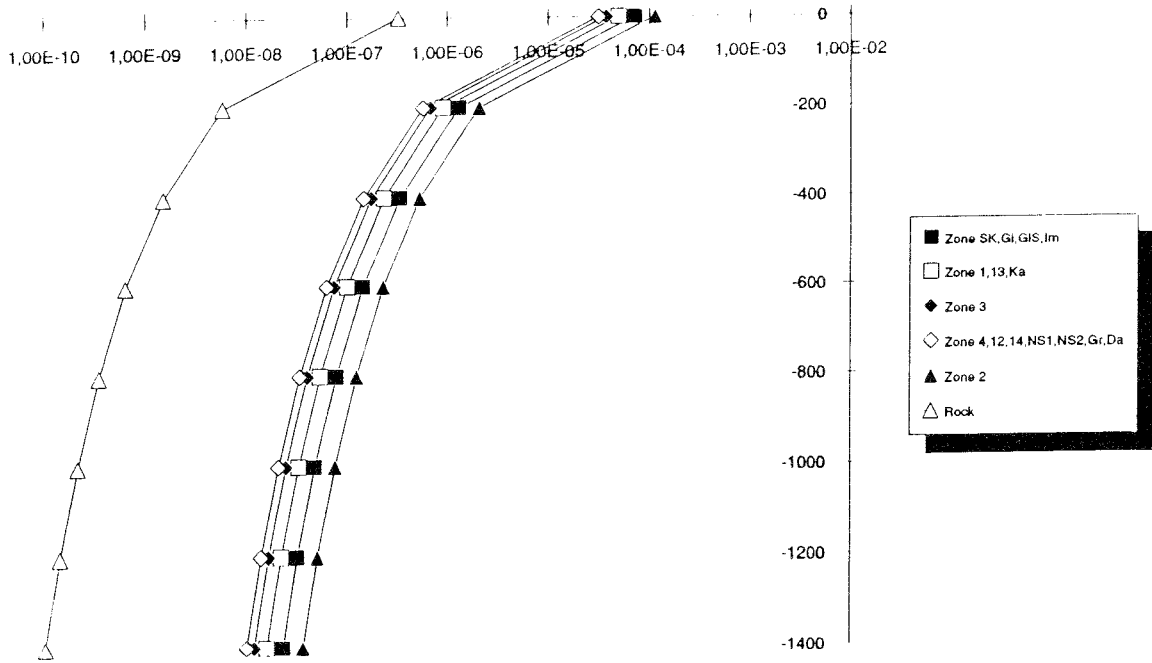


Figure 2.4c Depth dependence of rock mass conductivity and fracture zone conductivities for Case X36RM.

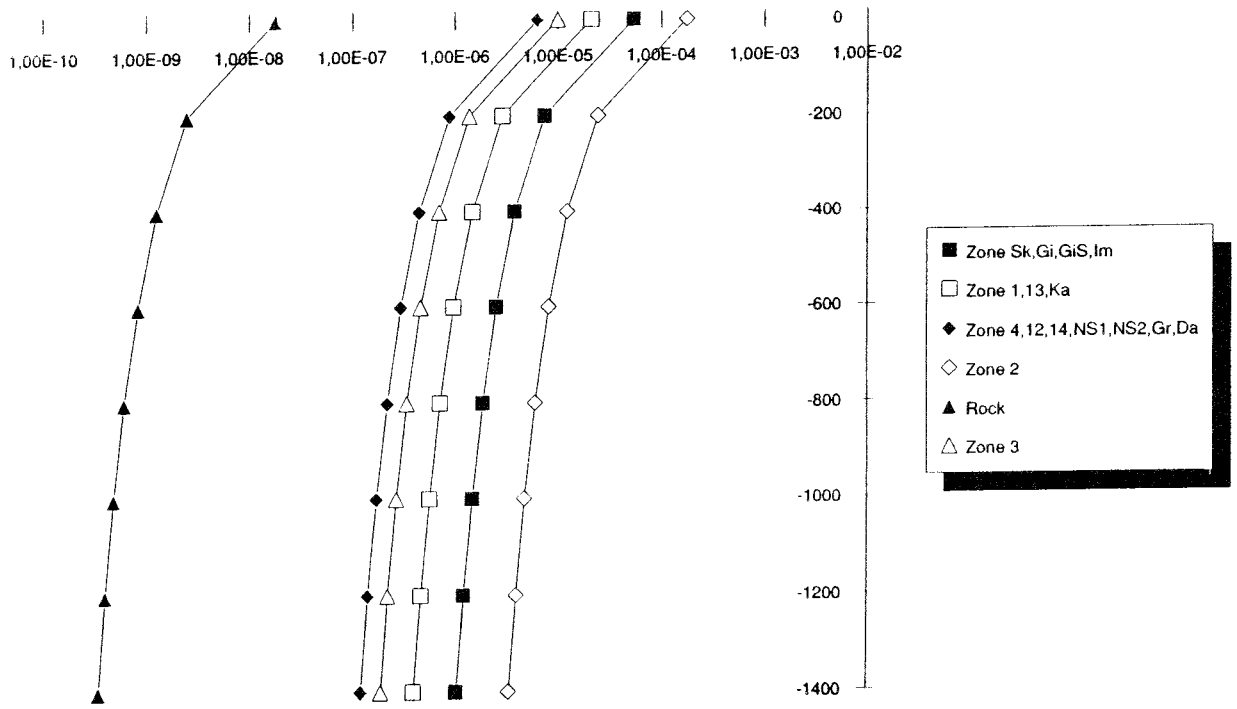


Figure 2.4d Depth dependence of rock mass conductivity and fracture zone conductivities as considered within the KEM1-study.

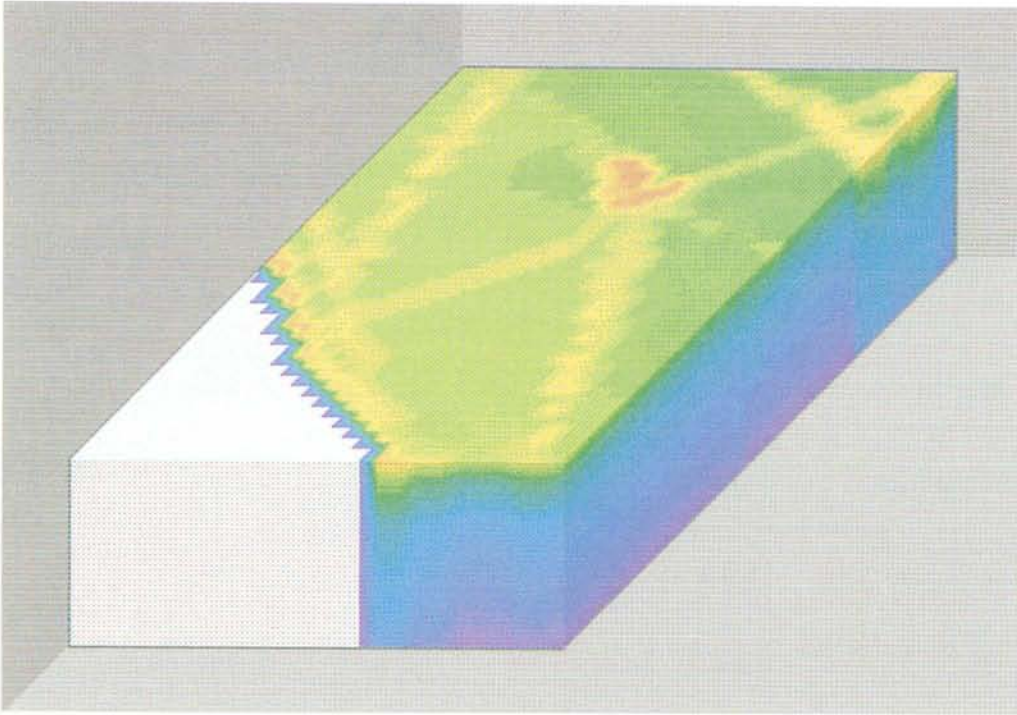


Figure 2.5a *Logarithmic hydraulic conductivities for Case X36 at a level of $z=0$ m. The conductivity decreases with increasing darkness of the colours.*

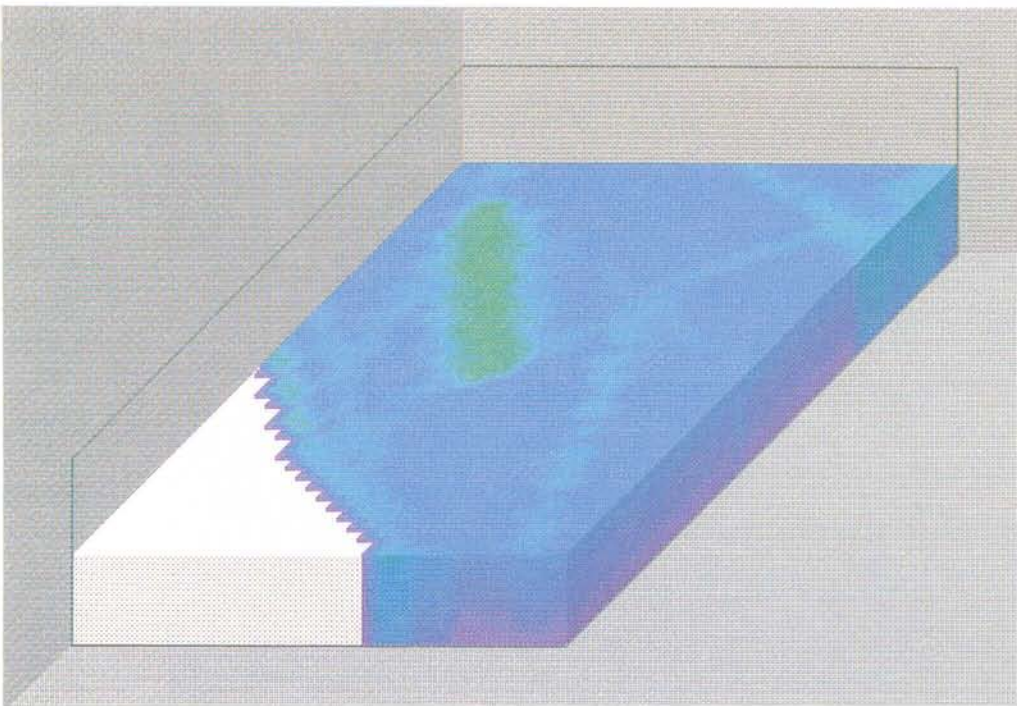


Figure 2.5b *Logarithmic hydraulic conductivities for Case X36 at a level of $z=-300$ m. The conductivity decreases with increasing darkness of the colours.*

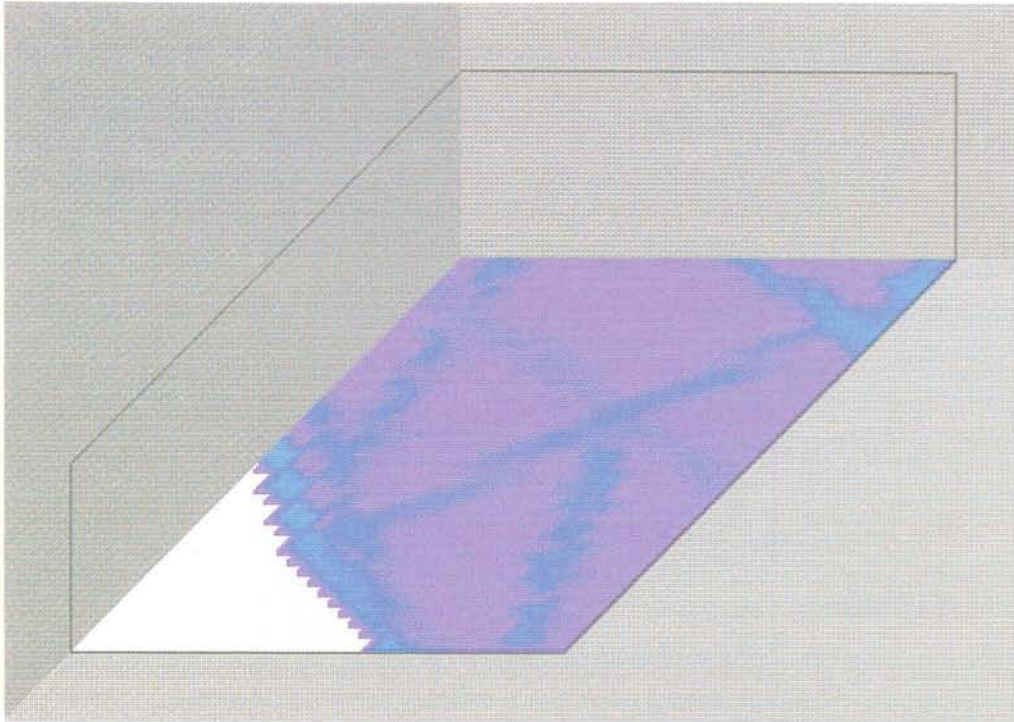


Figure 2.5c Logarithmic hydraulic conductivities for Case X36 at a level of $z = -600$ m. The conductivity decreases with increasing darkness of the colours.

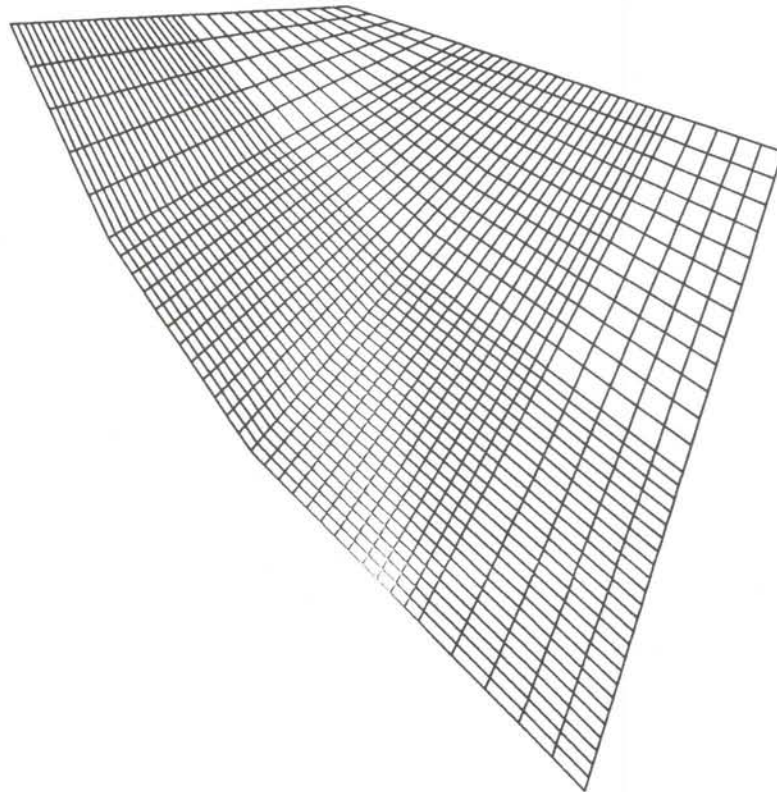


Figure 2.6 Top view of the finite element mesh that was generated for all the cases; the vertical discretisation differs for Cases X36V3 and X36V4 compared to the remaining cases.

3. Modelling Results

The evaluation for the modelled cases comprises the distribution of hydraulic head in a vertical cross-section, particle tracking with particles released within the repository area at $z=-600$ m, contoured flux distribution over the local scale block at repository level ($z=-600$ m), and frequency distribution of the fluxes over the local scale block at repository level. In addition to this, a 3D perspective colour plot illustrating the pressure field for Case X36 is shown, as well as the distribution of hydraulic head at $z=0$ m for the same case. Some figures have been moved to Appendix B in order to reduce the volume of the main part of the report.

The modelling results for Case X36 are discussed in Section 3.1, while the parameter variations are discussed in Section 3.2. Thus, the modelling results for Cases X36FR and X36RM are discussed in Section 3.2.1, the discussion on Cases X36V1, X36V3, and X36V4 is held in Section 3.2.2, and finally the results for Cases X36V2 and X36IM are discussed in Section 3.2.3. The presentation of results in the current text is somewhat more detailed for Case X36.

3.1 The Base Case (Case X36)

Pressure distribution

Figure 3.1 shows a 3D perspective colour plot of the calculated pressure field. The lilac part in the right-most part of the figure corresponds to a location where zone 1 intersects with the Giboda zone. The jagged boundary in the left-most part of the figure corresponds to zone 14. The three levels that are cut out are located at $z=-100$ m, $z=-300$ m, and $z=-600$ m. The plot illustrates that the solution obtained from NAMMU seems to have yielded rather a smooth pressure field, reflecting both peaks and dips in groundwater table. Furthermore, one may notice that there is quite a sharp interface between the greenish areas and the bluish ones, the latter representing a major discharge area. For comparison, the pressure distribution at a level of $z=0$ m is shown in Figure 3.2. One may notice that the peak as seen in the south-most part in Figure 3.1 corresponds to the hilly area directly south of the local scale block as indicated in Figure 3.2.

Figure 3.3 shows the distribution of hydraulic head in a vertical cross section crossing the local scale block entirely from south-west to north-east. The gradient is somewhat lower in the two right-most thirds of the plot with a predominant horizontal flow, whereas the left-most third shows areas with a higher gradient, mainly caused by the presence of the recharge area above zone 2.

Particle Tracking

Figure 3.4 and 3.5 show the horizontal and one vertical projection for Case X36. The location of the release points are shown in Figure 3.4. The figures show that the discharge takes place way up north in the Imundbo zone, into which all the particles enter. The flow paths start with a downward movement which is caused by the suction from zone 2, and by the fact that the area around the repository is a recharge area (see also Figure 3.3). The vertical projection onto the yz -plane also shows that once the particles enter the Imundbo zone, they follow the zone until they are discharged at ground level in the northern part of the domain.

The vertical projection of the pathlines on to the xz -plane is shown in Appendix B as Figure B1.

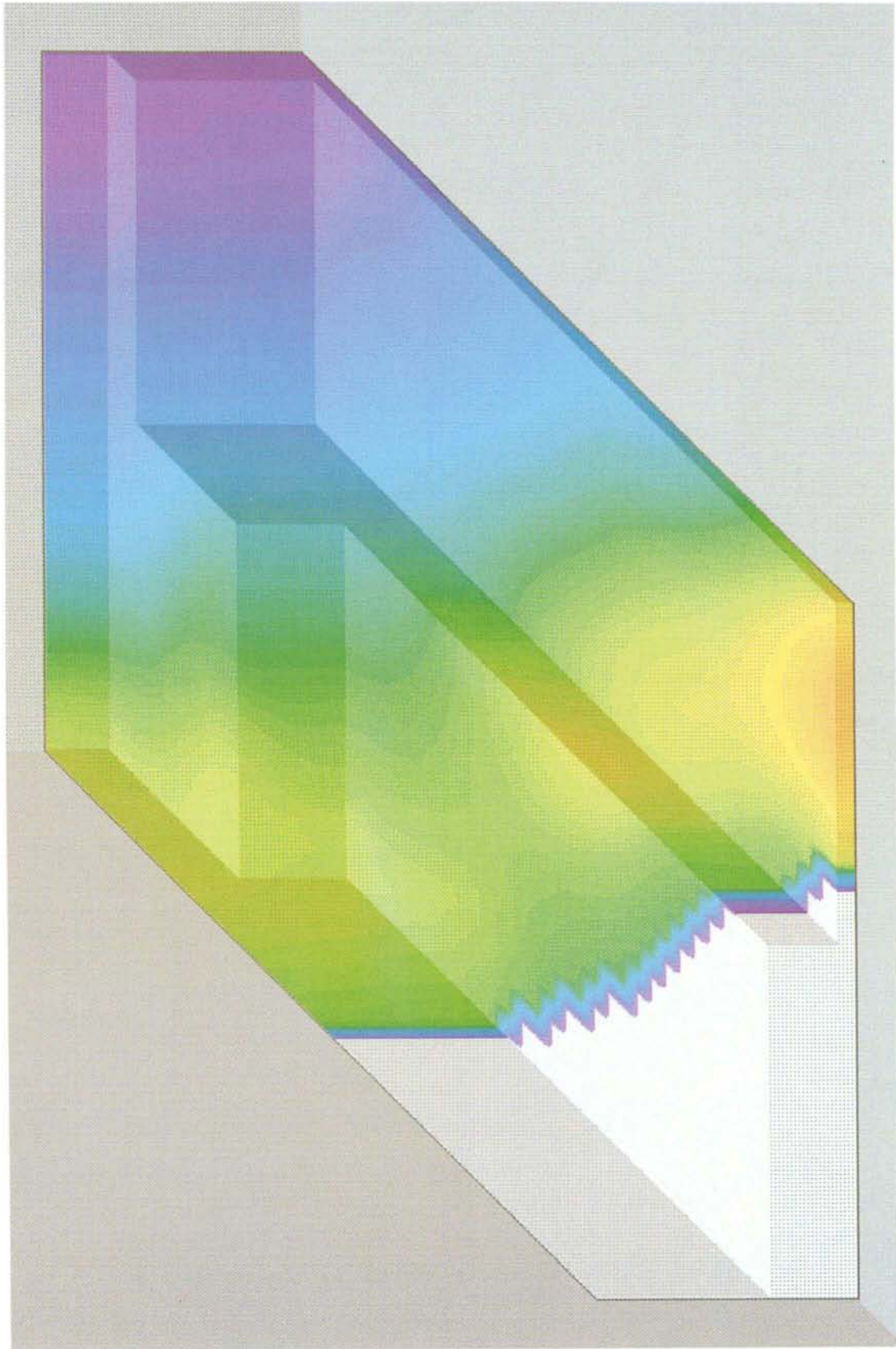


Figure 3.1 3D perspective plot illustrating the calculated pressure field for Case X36. The pressure decreases with increasing darkness of the colours.

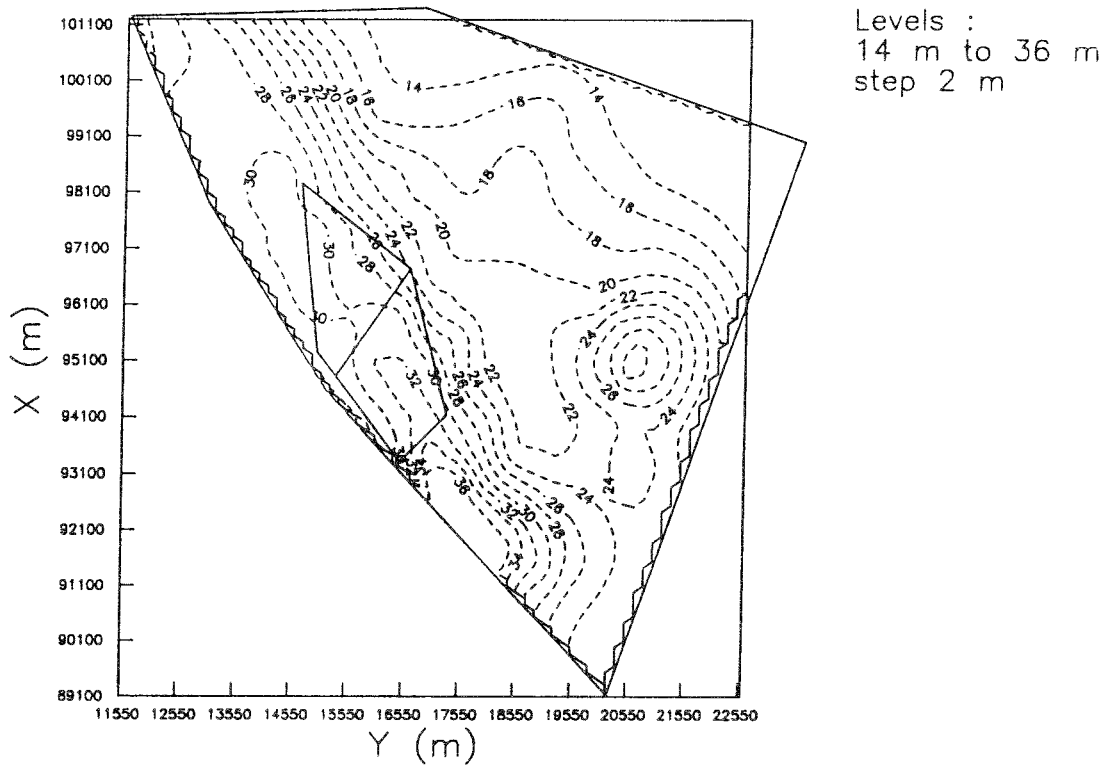


Figure 3.2 Distribution of hydraulic head at $z=0$ m for Case X36, see also Figure 2.1.

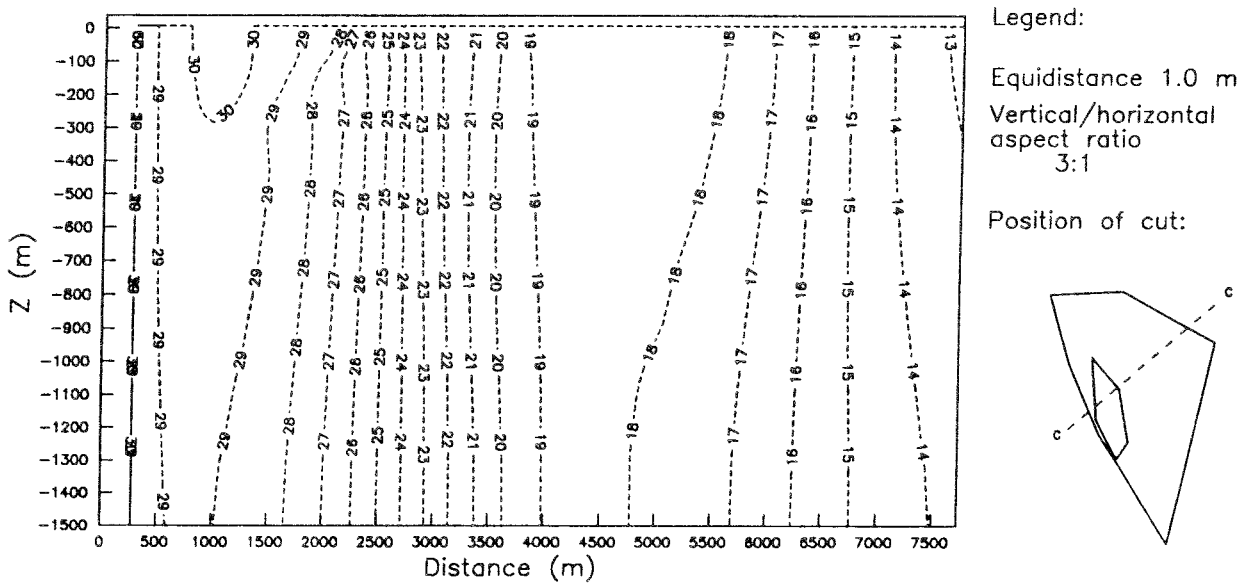


Figure 3.3 Distribution of hydraulic head in a vertical cut for Case X36.

Table 3.1 contains a collection of pathline data in terms of travel times and travel lengths for the generated particle tracks. The table shows that the travel lengths are of about the same order of magnitude for all particles. The differences in travel lengths correspond to the difference in distance from the release point to the Imundbo zone, so that the particles closest to this zone also have the shortest travel lengths. The particle track that deviated most from the others is particle 8, which has a travel length 300 m longer than any other as a result of it being released in the recharge area in the local scale block (see also Figure 3.3). The shortest travel time is obtained for particle 3, which also is the one released closest to the Imundbo zone.

Table 3.1 Accumulated travel times (ACT) in years, and accumulated travel lengths (ACL) in metres for Case X36. The particles were released at 600 m depth. A flow porosity of 0.0001 has been assumed when travel times were calculated.

Path no	ACT	ACL
1	485	5600
2	250	5580
3	170	5880
4	265	5780
5	350	5890
6	540	6050
7	550	6140
8	1000	6460

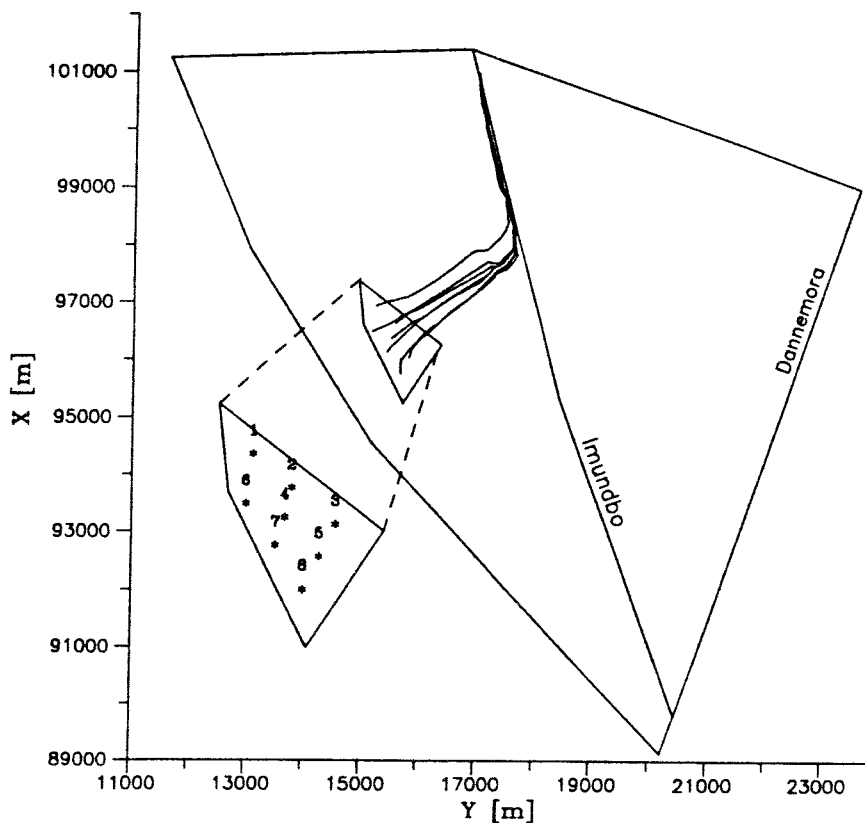


Figure 3.4 Horizontal view of pathlines for Case X36.

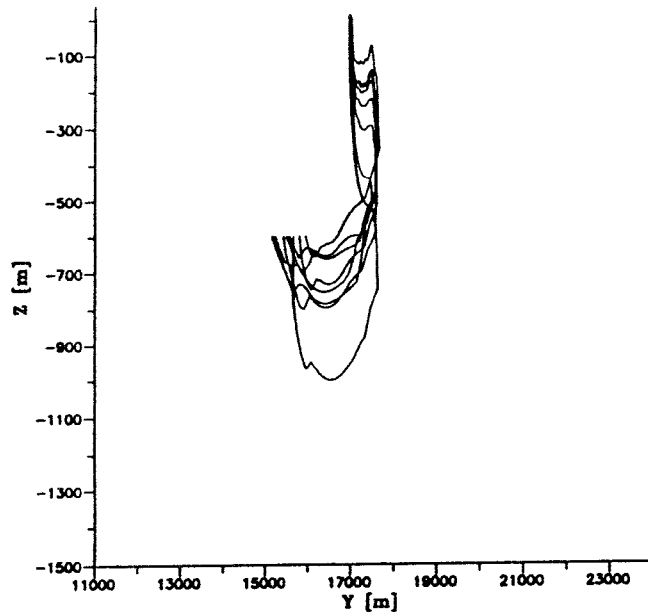


Figure 3.5 Vertical view of pathlines (yz-plane) for Case X36.

Flux distribution

Figure 3.6 shows the contoured flux distribution for Case X36 at $z=-600$ m. Typical values in the repository area are in the range $0.5-1.0 \cdot 10^{-3} \text{ m}^3/\text{m}^2/\text{year}$ with the higher values preferably in the vicinity of zone 4. Representative values for the southern block are about $1 \cdot 10^{-3} \text{ m}^3/\text{m}^2/\text{year}$. Figure 3.7 shows the frequency distribution of the fluxes over the same area as the contoured one in Figure 3.6. The median value is roughly $0.001 \text{ m}^3/\text{m}^2/\text{year}$, while the upper quartile corresponds to almost about $0.002 \text{ m}^3/\text{m}^2/\text{year}$.

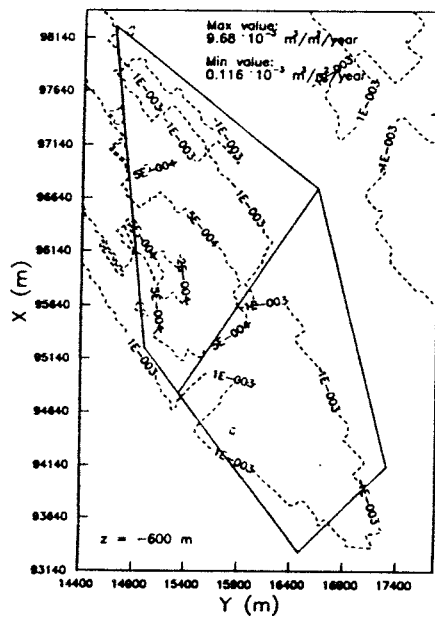


Figure 3.6 Contoured flux distribution ($\text{m}^3/\text{m}^2/\text{year}$) at repository level for Case X36.

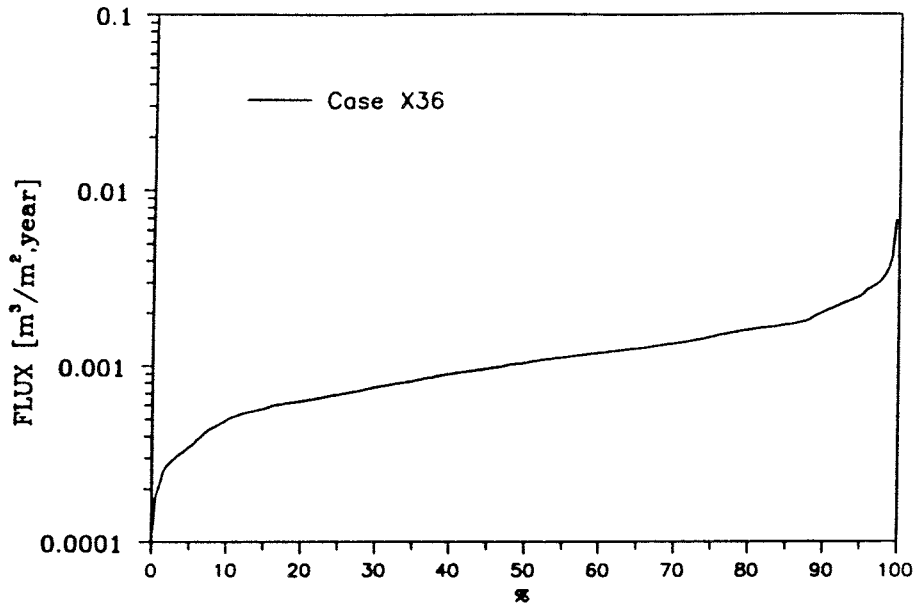


Figure 3.7 Cumulative flux distribution ($m^3/m^2/year$) at repository level for Case X36.

3.2 Parameter Variations

3.2.1 Sensitivity to Contrasts in Hydraulic Conductivity (Cases X36FR and X36RM)

The presentation comprises particle tracking and flux distribution. For Case X36FR, the figures showing the distribution of hydraulic head and the vertical (xz-plane) projection of the pathlines are shown in Appendix B, see Figures B2 and B3, respectively. Correspondingly, the figures for Case X36RM showing the hydraulic head distribution, pathlines, and the contoured flux distribution are shown in Appendix B as Figures B4, B5-B7, and B8, respectively. For a full description of the features and aims of the cases presented below, see Chapter 2.

Particle Tracking

Figures 3.8 and 3.9 show the horizontal and one vertical projection for Case X36FR for particles released at repository level with positions according to Figure 3.8. This figure shows that the discharge takes place at about the same position as for Case X36, see Figure 3.4. However, the two vertical projections reveal that an increased fracture zone conductivity can play an important role, not only in terms of faster travel paths, but also in terms of preferential pathways. The figures show that the water particles take an initial downward movement to be followed by rather a steep upward travel to a peak at a level of about $z=-200$ m. The position of this peak corresponds to the intersection between zones 1, 2, 3 and 4; see Figure 1.1. The conductivity of the same fracture zones in Case X36 was not high enough to have the water particles raised in the same manner. Once this intersection has been passed, the particles move downward to the approximate location of the intersection between zones 1, Giboda and Giboda South. From here, the particles move upward until the local topography predominates and pushes the particles towards the north, so that they finally are discharged close to the northern model boundary.

In Case X36RM, the particles take about the same paths from the repository as in Case X36. As can be seen in Table 3.2, the travel lengths are roughly the same as for Case X36. However, the travel times have been affected rather substantially by the reduced rock mass conductivity. The mean travel time (highest and lowest values omitted) is roughly 1060 years, which is about twice the value for Case X36.

A comparison between Table 3.1 and Table 3.2, shows that the travel lengths have been increased with roughly 10% as an average for Case X36FR, whereas the increased contrast in conductivity between rock mass and the fracture zones for Case X36FR made the travel times be about 70% shorter compared to Case X36. The increased travel lengths are probably due to the vertical movement around the intersection between zones 1, 2, 3 and 4.

Table 3.2 Accumulated travel times (ACT) in years, and accumulated travel lengths (ACL) in metres for Case X36FR and Case X36RM. The particles were released at 600 m depth. A flow porosity of 0.0001 has been assumed when travel times were calculated.

Case:	X36FR		X36RM	
Path no	ACT	ACL	ACT	ACL
1	119	6430	320	5870
2	81	6440	352	5630
3	59	6300	488	5540
4	109	6530	1405	5920
5	98	6520	856	5900
6	139	6950	1284	6140
7	182	6710	1979	6170
8	472	7040	2438	6370

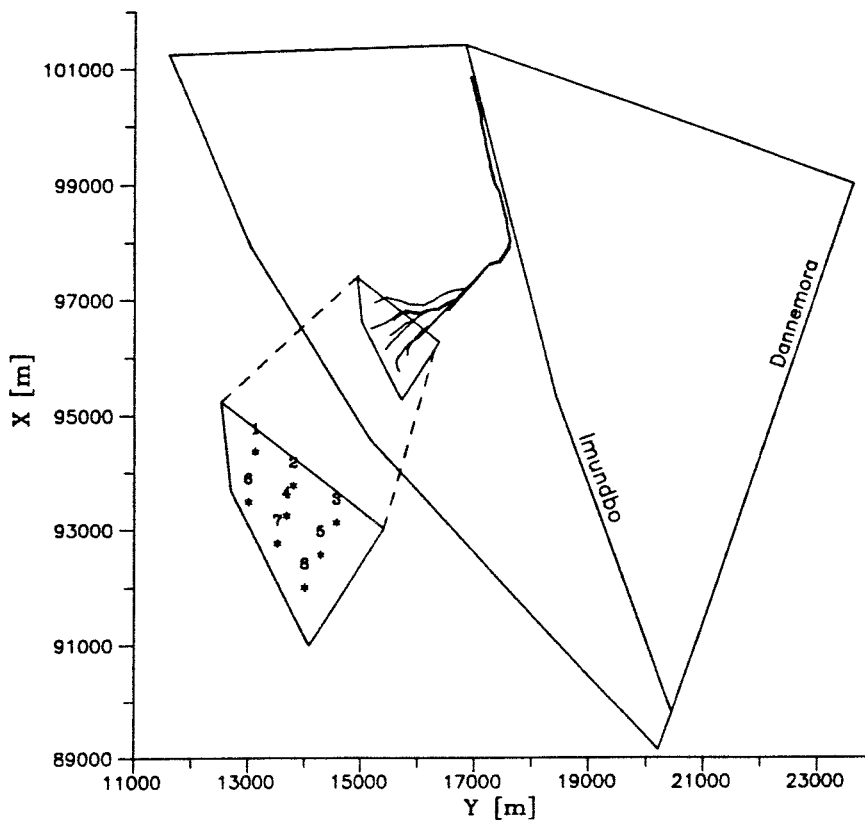


Figure 3.8 Horizontal view of pathlines for Case X36FR.

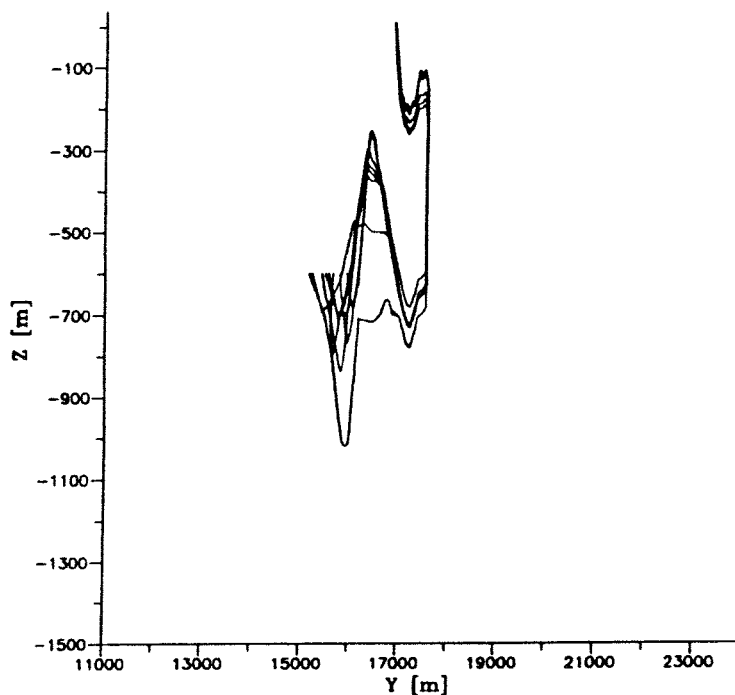


Figure 3.9 Vertical view of pathlines (yz-plane) for Case X36FR.

Flux Distribution

Figure 3.10 shows the contoured flux distribution for Case X36FR. Representative values are about the same as for Case X36, i.e. about $0.5-1.0 \cdot 10^{-3} \text{ m}^3/\text{m}^2/\text{year}$; also here with a tendency with the higher value in the vicinity of zone 4. Figure 3.11 illustrates the accumulated flux distribution for Case X36FR and Case X36RM, for comparison with the results of Case X36 included.

The median value for the flux is about the same for Case X36FR as for Case X36, while the upper quartile is about three times higher due to the higher fracture-zone conductivity. The total range between the lowest and the highest flux values is significantly larger for Case X36FR than for Case X36.

For Case X36RM, the lower rock mass conductivity has caused a corresponding lowering of the median flux. The highest flux values in Case X36RM are similar to the highest values calculated for Case X36.

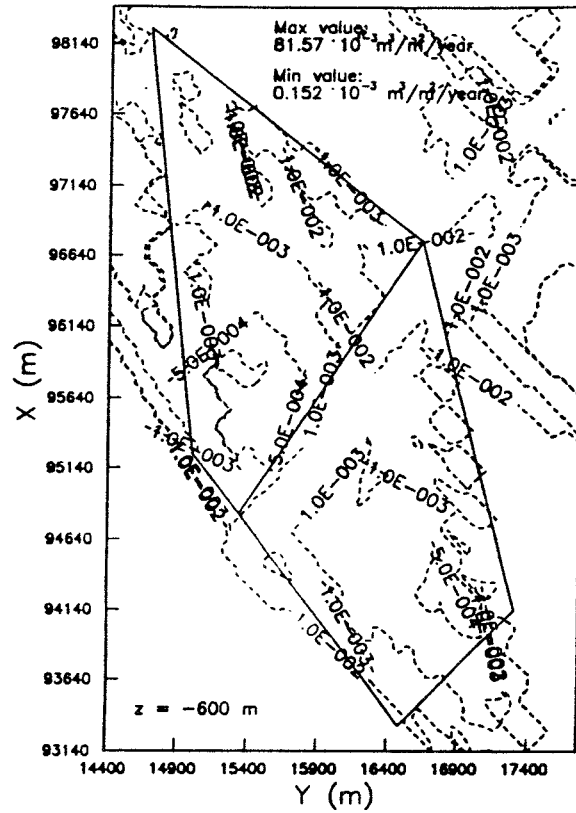


Figure 3.10 Contoured flux distribution ($\text{m}^3/\text{m}^2/\text{year}$) for Case X36FR.

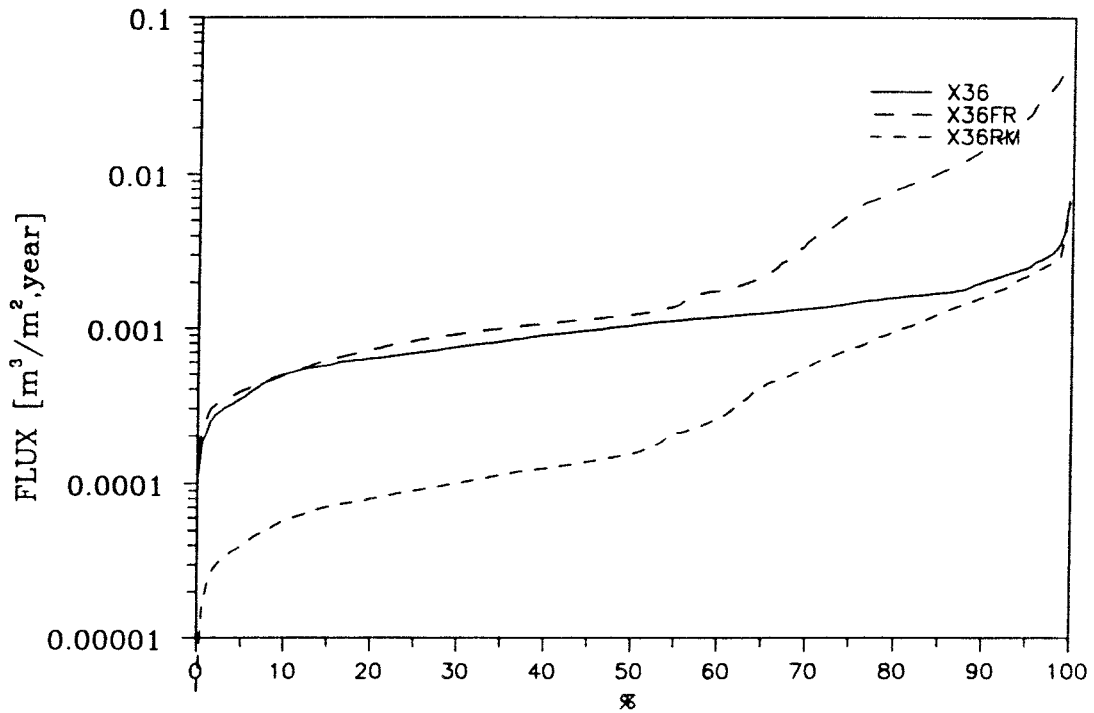


Figure 3.11 Cumulative flux distribution ($\text{m}^3/\text{m}^2/\text{year}$) for Cases X36, X36FR and X36RM.

3.2.2 Sensitivity to Major Permeable Sub-Horizontal Fracture Zones (Cases X36V1, X36V3, X36V4)

For a full description of the features and background of the calculation cases, see Chapter 2. This presentation will be focussed on particle tracking and flux distribution at repository level, and also on the distribution of hydraulic head for Case X36V3. The figures for Case X36V1 showing the distribution of hydraulic head, vertical projections of pathlines, and the contoured flux distribution are shown in Appendix B, see Figures B9, B10-B12 and B13, respectively. The figures for Case X36V3 showing the vertical projections of the pathlines, and the contoured flux distribution are shown in Appendix B as Figures B14-B15 and B16, respectively. The figures showing the distribution of hydraulic head, the vertical projections of pathlines, and the contoured flux distribution are shown in Appendix B as Figures B17, B18-B19 and B20, respectively.

Pressure Distribution

Figure 3.12 shows the distribution of hydraulic head in a vertical cross-section. The introduction of the new zone 2u has obviously reinforced the area above the repository as being a recharge area. If comparing this figure with Figure 3.3 (Case X36), the curvature of the isopotentials is stronger in the repository area (corresponding to about 500 m to 2000 m in distance on the abscissa), where the 29m-curve and the 28m-curve are affected. The 2u-zone has apparently transmitted potentials from the surface to the lower levels and thus created an even stronger recharge area. However, pressure is a first order entity and known not to be a very sensitive measure in this context, implying only a local influence in this figure. The right-most part of the figure seems to be left more or less unaffected by the zone, although it extends over a large part of the modelled domain.

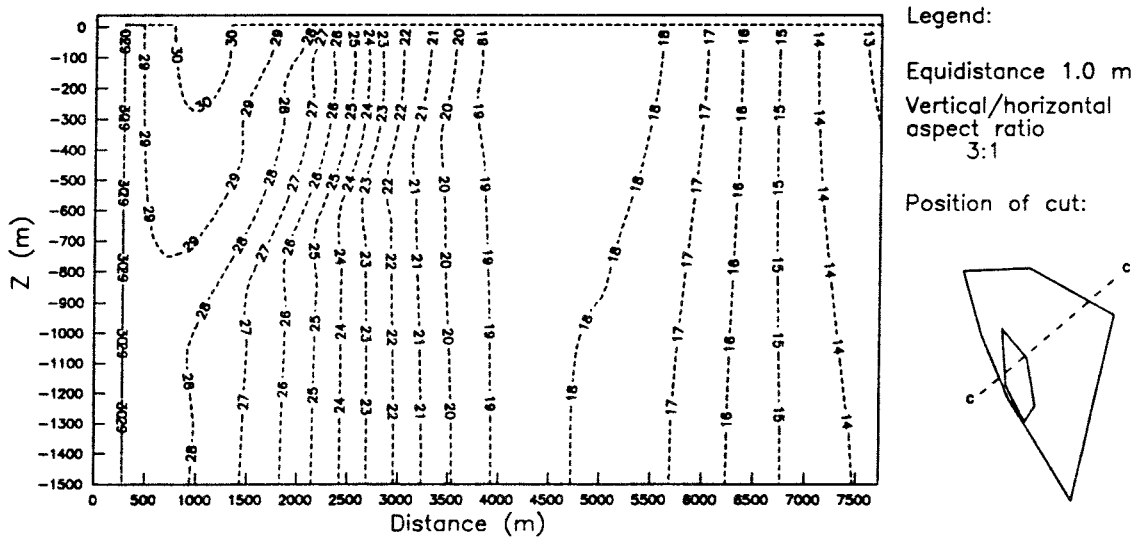


Figure 3.12 Distribution of hydraulic head in a vertical cut for Case X36V3.

Particle Tracks

Apart from minor differences, the flow paths and discharge point are roughly the same for Case X36V1 as for Case X36. However, the results for Case X36V3 and Case X36V4 indicate rather a strong influence from a major sub-horizontal zone below the repository.

Figures 3.13 and B14-B15 (Appendix B) show the horizontal and vertical projections of the particle tracks for Case X36V3. These figures reveal that the 2u zone affects the travel paths strongly. The particles are mainly discharged in the Imundbo zone, but earlier than in Case X36. A couple of the particles are discharged in the vicinity of the intersection between the Imundbo zone and the Giboda S zone, whereas the remainder are discharged a distance farther away in the Imundbo zone. Figures B14-B15 reveal that the transport to the discharge point takes place in the 2u zone. It is also interesting to notice that the particles are directed almost instantly vertically to the 2u zone from the release points. This is of course a consequence of the reinforced recharge caused by the 2u zone.

Figure 3.14 shows the horizontal projection of pathlines for Case X36V4. As can be seen, the point of discharge is still in the northern part of the Imundbo zone. However, as shown in Figures B18-B19 (Appendix B), the transport from the release points is directly vertical down to the 2u zone for further transport in this zone to the Imundbo zone, i.e. the whole transport, except for the initial part, takes place in fracture zones.

The travel times and travel paths are collected in Table 3.3. Although it is not a stringent statistical measure, some sort of mean travel time and travel length could be calculated for the particle tracks by simply calculating the mean travel time and travel length excluding the lowest and highest values. The resulting mean travel time for Case X36V1 is about 520 years with a mean travel length of about 5890 m. Corresponding values for Case X36 are 410 years and 5890 m. Since the travel lengths are the same in both cases, one could assume that the particles in Case X36V1 take steeper travels to the surface than in Case X36, or that the part of the travel paths that takes place in zone 2 for Case X36 now is transported in the rock mass. The travel times are about 30% shorter for Case X36V3 than for Case X36, while the travel lengths were about the same for both cases.

Almost the whole transport for Case X36V4 takes place in fracture zones as indicated above, which gives a fast transport, see Table 3.3. The 2u zone has affected the flowpath lengths to a limited degree, but the effect on the travel times is significant. The mean travel times and travel lengths are 65 years and 5870 m, respectively (the lowest value and particle 8 omitted, since particle 8 was aborted due to numerical difficulties). In conclusion, the 2u zone has affected the travel times strongly in the absence of zone 2, which confirms the utmost importance of zone 2 acting as a "barrier" for vertical transport of water to the deeper parts of the domain.

Table 3.3 Accumulated travel times (ACT) in years, and accumulated travel lengths (ACL) in metres for Cases X36V1, X36V3, and X36V4. The particles were released at 600 m depth. A flow porosity of 0.0001 has been assumed.

Case:	X36V1		X36V3		X36V4	
Path no	ACT	ACL	ACT	ACL	ACT	ACL
1	466	5510	406	5510	91	5420
2	263	5510	296	5540	39	5450
3	255	5540	249	5630	42	5740
4	431	5890	339	3490	49	5890
5	457	6010	339	5980	36	6070
6	618	6120	450	5960	100	5920
7	875	6250	450	3670	66	6170
8	1690	6770	837	6410	59	6520

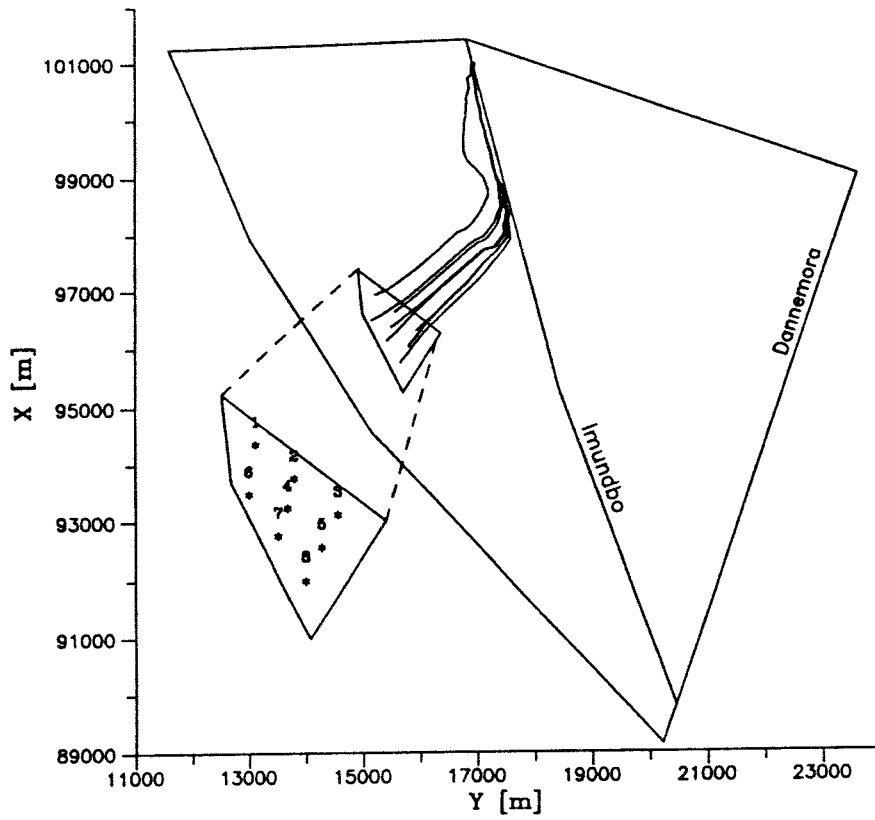


Figure 3.13 Horizontal view of pathlines for Case X36V3.

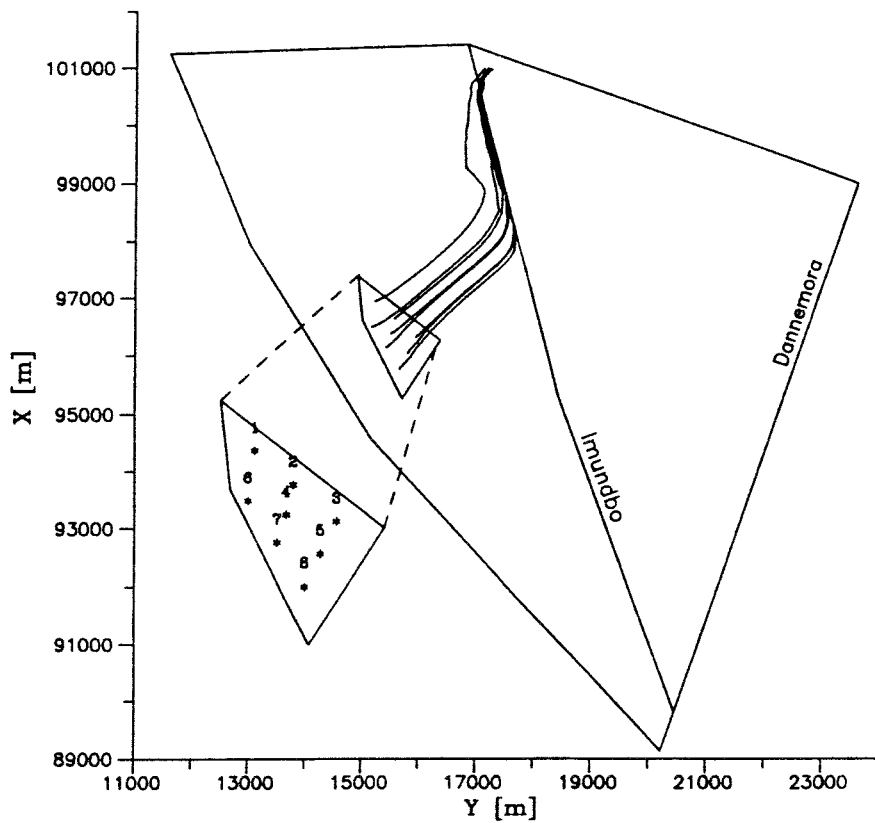


Figure 3.14 Horizontal view of pathlines for Case X36V4.

Flux Distribution

The frequency of the flux distribution at repository level is shown in Figure 3.15 for the three cases; for comparison the curve for Case X36 is also included. The figure indicates that the differences occurring due to the absence of zone 2 are negligible when zone 2u is not modelled (Case X36V1). The median value is about 0.0011-0.0013 $\text{m}^3/\text{m}^2/\text{year}$ (10-30% higher than for Case X36), while the upper quartile is about the same as for Case X36, i.e. about 0.0015 $\text{m}^3/\text{m}^2/\text{year}$.

The modelling of zone 2u in the presence of zone 2 (Case X36V3) affects the fluxes at repository level only slightly; the bulk of the values are in the range 0.001-0.002 $\text{m}^3/\text{m}^2/\text{year}$ (lower and upper quartile) with median value of about 0.0015 $\text{m}^3/\text{m}^2/\text{year}$. The fluxes at repository level are thus a bit higher for Case X36V3, which mainly depends on the vertical flow beneath zone 2 and above zone 2u, caused by the drainage of water to zone 2u.

The results for Case X36V4 in the figure reveal that the 2u zone has affected not only the transport times in the zone, but also the fluxes at repository level, compared to Case X36. Apparently, the introduction of zone 2u when zone 2 is not modelled has changed the picture rather substantially. The lower quartile in the figure is about 0.001 $\text{m}^3/\text{m}^2/\text{year}$, while the upper quartile is about 3 times that high; median value is roughly 0.002 $\text{m}^3/\text{m}^2/\text{year}$. The large areal coverage of the zone is also illustrated by the relatively large increase in the high end of the curve, which could be seen as the influence of flow in the fracture zones in general and in zone 2u in particular.

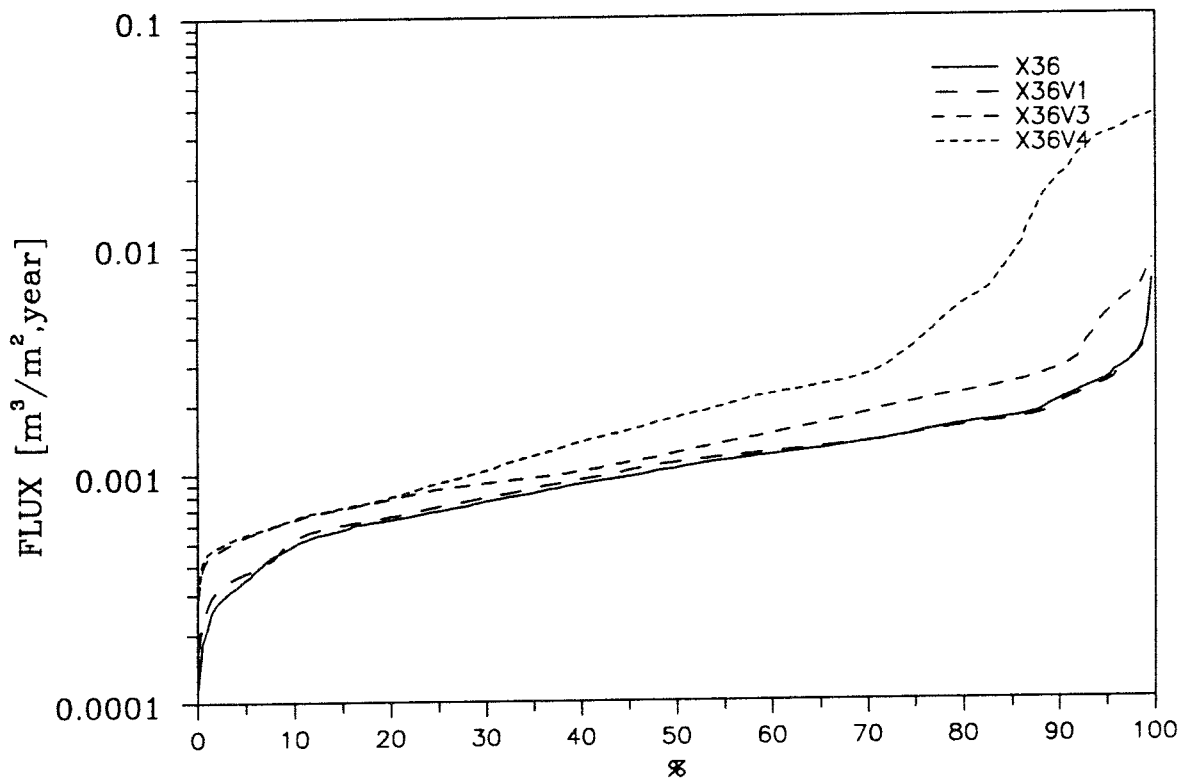


Figure 3.15 Cumulative flux distribution ($\text{m}^3/\text{m}^2/\text{year}$) for Cases X36, X36V1, X36V3 and X36V4.

3.2.3 Confidence in the Location of the Discharge Area – Imundbo (Cases X36V2 and X36IM)

The two cases presented below were analysed in order to investigate the confidence in stating that the Imundbo zone can be regarded as the major discharge area for radio-nuclides released from the potential repository. The features and aims of the cases are described in Chapter 2.

The presentation is focussed on particle tracking and the cumulative distribution of the fluxes at repository level. The figures for Case X36V2 showing the distribution of hydraulic head, vertical projection of pathlines in the xz-plane, and the contoured flux distribution are shown in Appendix B, see Figures B21, B22 and B23, respectively. The figures for Case X36IM showing the distribution of hydraulic head, the vertical projections of pathlines, and the contoured flux distribution are shown as Figures B24, B25-B26, and B27, respectively.

Particle tracking

The horizontal and vertical projections (yz-plane) of the particle tracks for Case X36V2 are shown in Figures 3.16 and 3.17, respectively. These figures indicate that the discharge still takes place in the area of the Imundbo zone, but at a location much closer to the repository than was the situation for Case X36. Now that the Imundbo zone is modelled as rock mass, the particles tend to be discharged at the surface in the vicinity of the intersection between the Imundbo zone and the Giboda S zone. This leads to two conclusions: *a)* the discharge area is pronounced enough to behave as a discharge area also without the Imundbo zone, but the point of discharge has been moved southward, and *b)* other features than the Imundbo zone could act as discharge points, e.g. the Giboda S zone, preventing the particles from reaching the north-east corner of the domain.

The horizontal projection of the pathlines for Case X36IM is shown in Figure 3.18. The flow paths seem to be affected only to a minor degree by the sloping Imundbo zone. The pathlines appear to run beside the Imundbo zone as the zone slopes, and the figure shows the Imundbo zone as it appears on the ground surface. The discharge point is roughly the same as for Case X36.

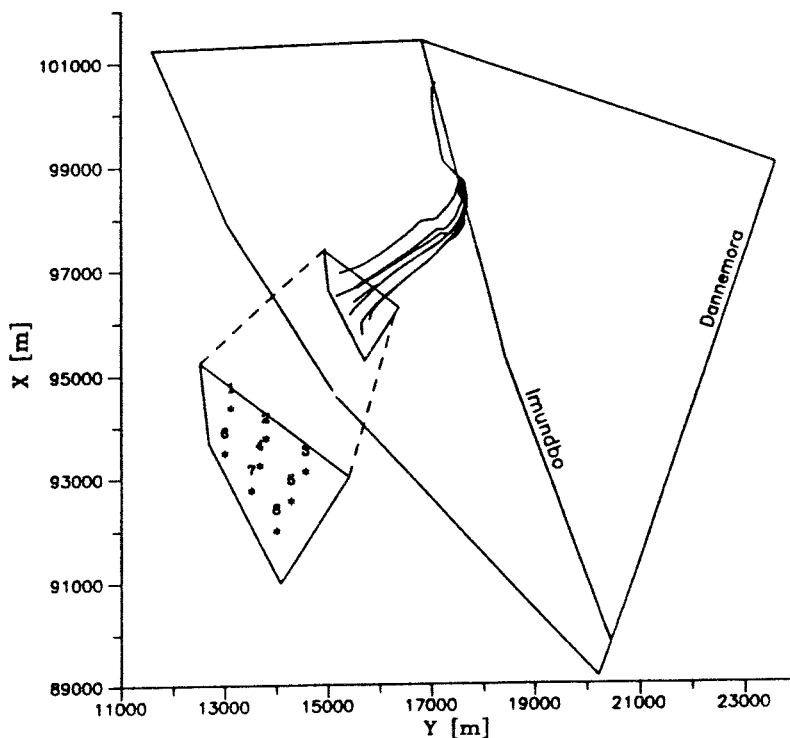


Figure 3.16 Horizontal view of pathlines for Case X36V2.

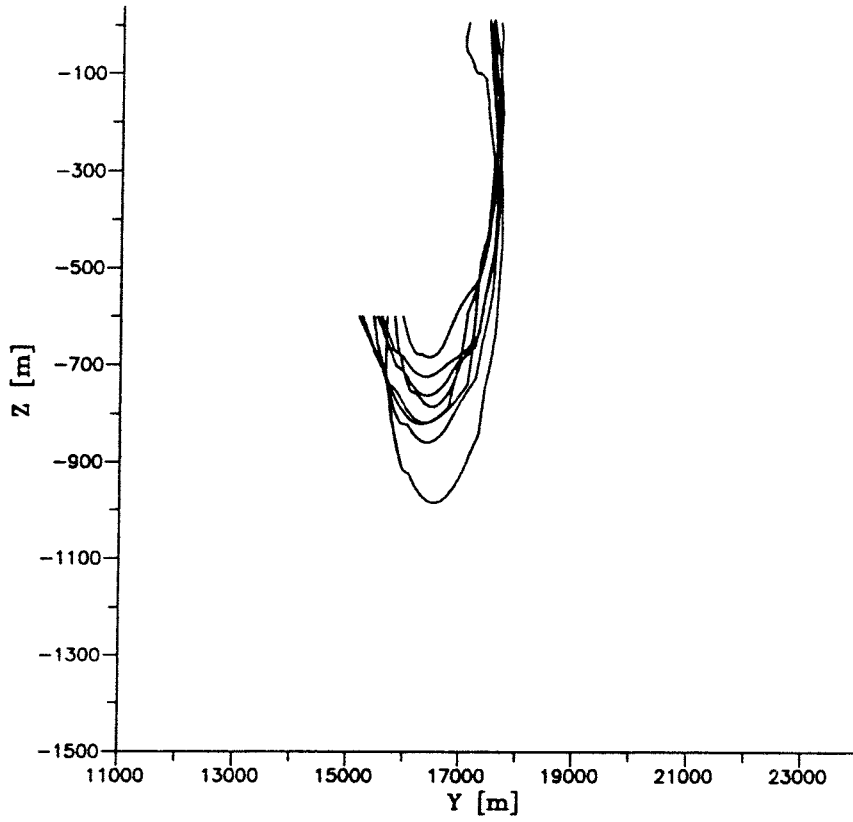


Figure 3.17 Vertical view of pathlines (yz-plane) for Case X36V2.

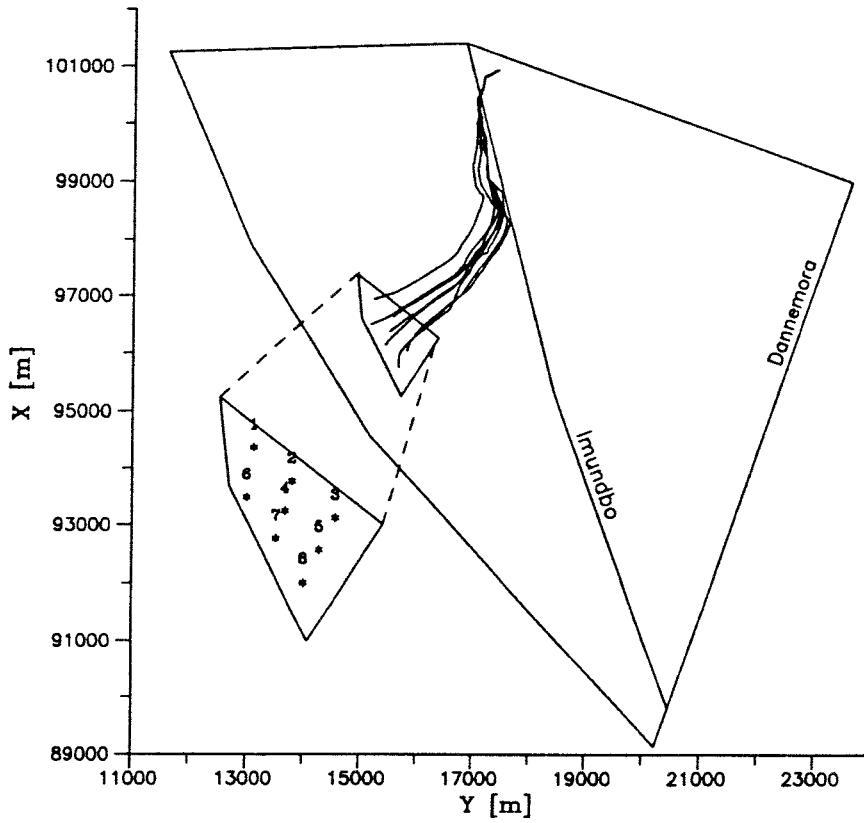


Figure 3.18 Horizontal projection of pathlines for Case X361M.

The travel times and travel lengths for the two cases are shown in Table 3.4 below. The mean travel times and travel lengths for Case X36V2 are 470 years and 3940 m, respectively (lowest and highest values omitted). The somewhat longer travel times compared to Case X36 are probably due to the lack of drainage from the Imundbo zone in this case, and the shorter travel lengths are naturally caused by the lack of a long and permeable transport path now that the Imundbo zone is modelled as rock.

The travel times are about twice as long for Case X36IM than for Case X36. This can be explained as follows: The inclination of the Imundbo zone transfers the hydraulic head at the top surface downwards, implying that the z-component of the gradient at repository level is directed downwards. This means that the particles are subjected to a suction vertically downwards and in the NE-direction, i.e. towards the discharge point. The deeper travel paths for Case X36IM, are the reason for the longer travel times compared to Case X36. This discussion is also confirmed by the vertical projections of the pathlines in Appendix B, where most pathlines go down to about z=-1100 m prior to their upward movement. Corresponding lowest z-coordinate for Case X36 is about 800 m below ground surface.

Table 3.4 Accumulated travel times (ACT) in years, and accumulated travel lengths (ACL) in metres for Case X36V2 and Case X36IM. The particles were released at 600 m depth. A flow porosity of 0.0001 has been assumed when the travel times were calculated.

Case:	X36V2		X36IM	
Path no	ACT	ACL	ACT	ACL
1	507	5290	809	5580
2	309	3220	698	5690
3	178	2900	523	5920
4	415	3690	780	6030
5	381	3510	796	6250
6	564	3910	1088	6140
7	647	4030	1123	6250
8	964	4410	1516	6750

Flux distribution

The frequency of the flux distributions are shown in Figure 3.19 for Cases X36V2 and X36IM; the curve for Case X36 is also included in the figure for the sake of comparisons. The results for Case X36V2 indicate that the model results in terms of fluxes at repository level seem to be more or less unaffected by the absence of the Imundbo zone, and so does the contoured flux distribution in Appendix B. The bulk of the values for this case is within a span of 0.0007-0.0015 m³/m²/year (lower and upper quartile), while the median value is about 0.001 m³/m²/year. The lack of difference is probably due to the relatively long distance between the Imundbo zone and the repository; the area over which the fluxes were calculated.

The results for Case X36IM are similar to those of Case X36 with only minor insignificant differences.

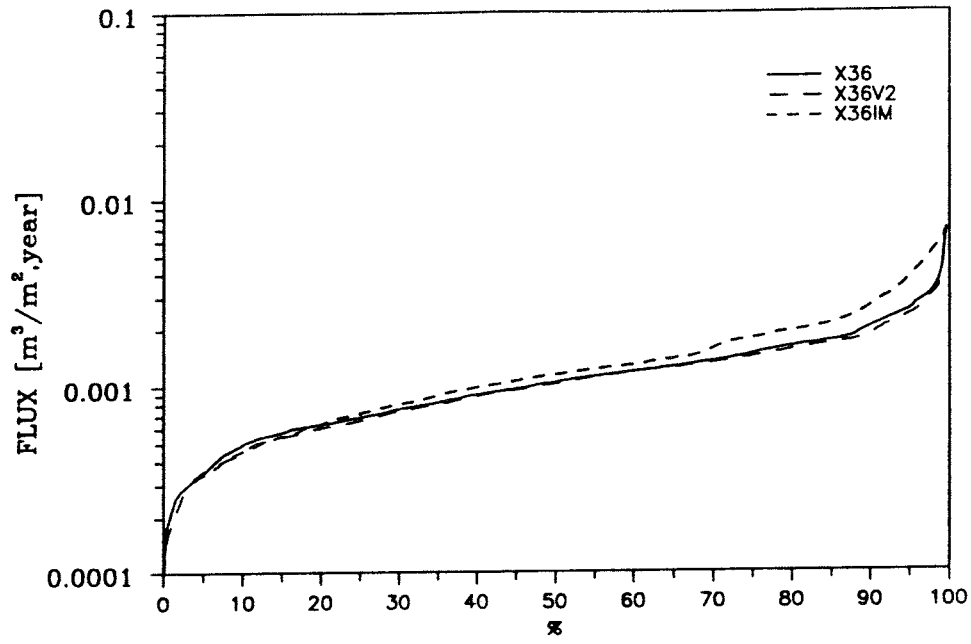


Figure 3.19 Cumulative flux distribution ($\text{m}^3/\text{m}^2/\text{year}$) for Cases X36, X36V2 and X36IM.

4. Summary and Conclusions

Eight cases have been studied within the project; the hydraulic conductivity distribution for all of them was based on an upscaling procedure (a so called regularisation) of packed-off bore hole sections with lengths of 2-3 m to an averaging length of 36 m. This was obtained as part of the input scheme to the HYDRASTAR-code. The procedure yielded contrasts in hydraulic conductivity between the rock mass and the fracture zones lower than that used in the previous analysis.

Seven calculation cases were performed in addition to the Base Case. They were focused on three main sources of uncertainty addressing the model sensitivity to conductivity contrasts and to the presence of major sub-horizontal fracture zones. In addition, the confidence of the location of the discharge area was analysed.

The Base Case (called Case X36) involved the modelling of the rock mass and fracture zones with a maximum conductivity contrast of a factor of about 35. The fluxes at repository level amounted to about $0.001 \text{ m}^3/\text{m}^2/\text{year}$ as a median value with a tendency to higher values in the vicinity of fracture zone 4. The upper quartile value was almost about $0.002 \text{ m}^3/\text{m}^2/\text{year}$. The travel times for water particles from the repository were about 450 years (a porosity of 0.0001) with average lengths of about 5500 m. The point of discharge was located just by the model boundary in the northern part of the modelled domain in the Imundbo zone.

The two cases addressing the sensitivity to conductivity contrasts (increased to a factor of 400, (zone 2 excluded), showed that the model is very sensitive to an increased fracture zone conductivity with a travel time reduction of 70% as a consequence. The fluxes at repository level were increased with roughly one order of magnitude at its most. The situation with an increased contrast by a reduced rock mass conductivity showed that the travel times are twice as high as for the Base Case, which of course depends on the increased residence time in the rock. The fluxes at repository level were reduced proportionally to the reduction of the rock mass conductivity.

The three cases dealing with the presence of major sub-horizontal permeable fracture zones, indicated a strong influence, particularly the situation with a generic zone (assumed undetected hitherto) below the repository without the presence of a similar zone above the repository. The latter acts a separator for vertical flow exchange between the regions above and below the zone. This case showed travel times that were reduced with about 85% (about 65 years as an average) compared to the Base Case, depending on a vertical downward transport from the repository to the sub-horizontal zone and a further transport in this zone to the model boundary. The two cases with the generic zone modelled showed median values being roughly twice as high as the other cases (about $0.002 \text{ m}^3/\text{m}^2/\text{year}$) and upper quartile values of about $0.003\text{-}0.006 \text{ m}^3/\text{m}^2/\text{year}$.

The discharge point for released water particles was rather well defined by the model for all cases studied; the major discharge collector was the Imundbo zone. The confidence in this statement was tested by treating the Imundbo zone as rock mass and by sloping the Imundbo zone 45° SW (towards the repository) in order to analyse the effects of an increased gradient at deeper depths. Both cases reinforced the impression that the area in the vicinity of the Imundbo zone was the major discharge area. However, the case with the Imundbo zone treated as rock mass made the particles be discharged closer to the repository, although the travel times to this discharge point was about the same as for the Base Case. The situation with the zone sloping indicated longer travel times than for the Base Case.

In conclusion, one could state that the point of discharge seems to be fairly certain. The area around the Imundbo zone acts as the major collector for water stemming from the repository. If the hydraulic properties of the Imundbo zone could be thought of as over-estimated, the area still acts as a discharge region, although the particles enter the top model boundary at a position located further south than when the Imundbo zone was modelled with fracture zone properties.

The fracture zone conductivities were assigned implicitly with an averaging technique so that the fracture zone properties were assigned to the finite elements that were crossed by the fracture zone planes, not necessarily coinciding with element borders. As a result of this procedure, peak values that usually are obtained with specific fracture zone elements were less pronounced. This conclusion holds for both travel times and flux values, and depends on that the fracture zone properties are averaged over a larger number of elements than with ordinary "specific fracture zone element technique".

A second source of uncertainty could be the fracture zone properties in a general sense. The results indicated that the model was rather sensitive to a substantially increased fracture zone conductivity compared to the Base Case. The fracture zone conductivities used in this study are significantly lower than those previously assumed (KEM1, 1991). The difference between the two data sets is that the data used in this study come from statistical analyses of measured data, while the data in the previous study were based partly on judgments. It is obvious that the difference between the data sets are of potential importance.

Perhaps the most serious source of uncertainty, is the situation when a fracture zone remains undetected, particularly if the zone is permeable and extends over large areas. This situation was found to be the most sensitive one that was studied within this project, since it affected not only the travel times from the repository but also the fluxes at repository level. The latter may in turn affect the efficiency of the engineered barriers in the proximity of the repository, and the presence of the permeable fracture zone provides means for a fast transport of the potentially dissolved radionuclides from the repository.

References

HARW1, 1979:

Rae J., P.C. Robinson, 1979,

"NAMMU: Finite-Element program for coupled heat and groundwater flow problems", Report AERE R-9610, U.K. Atomic Energy Research Establishment, Harwell Laboratory, United Kingdom.

HARW2, 1985:

Atkinson R., A.W. Herbert, C.P. Jackson, P.C. Robinson, 1985,

"NAMMU User Guide", Report AERE R-11364, U.K. Atomic Energy Research Establishment, Harwell Laboratory, United Kingdom.

KEM1, 1991:

Lindbom B, Boghammar A, 1991,

"Numerical groundwater flow calculations at the Finnsjön study site", SKB Technical Report 91-12, Swedish Nuclear Fuel and Waste Management Company, Stockholm, Sweden.

KEM2, 1989:

Grundfelt, B., A. Boghammar, H. Lindberg, 1989

"HYPAC User's Guide", SKB Working Report 89-22, Swedish Nuclear Fuel and Waste Management Company, Stockholm, Sweden.

KEM3, 1989:

Lindbom B, Lundblad K, Markström A, 1989,

"Initial Groundwater Flow Calculations at the SKI Reference Site", SKI Technical Report 89:2, Swedish Nuclear Power Inspectorate, Stockholm, Sweden.

SGAB1, 1991:

Andersson J-E, Nordqvist R, Nyberg G, Smellie J, Tirén S, 1991,

"Hydrogeological conditions in the Finnsjön area; Compilation of data and conceptual model", SKB Technical Report 91-24, Swedish Nuclear Fuel and Waste Management Company, Stockholm, Sweden.

SGAB2, 1991:

Tirén S, Geosigma AB, Uppsala, Sweden, Personal communication, 1991.

STAR, 1991:

Norman S, 1991,

"Verification of HYDRASTAR – A code for stochastic continuum simulation for groundwater flow", SKB Technical Report 91-27, Swedish Nuclear Fuel and Waste Management Company, Stockholm, Sweden.

List of Symbols

H	Heat source strength	(W/m ²)
K	hydraulic conductivity	(m/s)
T	common rock/fluid temperature	(K)
c	compressibility	(Pa ⁻¹)
c _p	specific heat	(J/K/kg)
g	gravity acceleration	(m/s ²)
k	permeability (intrinsic)	(m ²)
p	(total) fluid pressure	(Pa)
q	(Volumetric) flux, Darcy velocity	(m ³ /m ² /s), (m/s)
x,y,z	cartesian coordinates	(m)
Γ	dispersion coefficient	(m ² /s)
ε	flow porosity	(-)
η	dynamic viscosity of the fluid	(Pa·s)
φ	potential (piezometric level)	(m)
ρ	density	(kg/m ³)
(ρc _p) _a	average heat capacity of rock and fluid	(J/K/kg)
∇	gradient operator	

Overlying horizontal bar indicates vector entity.

Superscripts

f	fluid
r	rock

Subscripts

a	average value
d	dynamic
x,y,z	referring to (cartesian) direction

Appendix A

Documentation of files created and processed during the project

For each case the program sequence and input and output files used are listed. The outputfiles marked with a "*" are unique and have been saved. If not otherwise stated all files reside on /files/home/users/kemhl/0250 on SKB's Convex C220 computer.

For further information with regard to file-name conventions and the contents on the files referred to in this Appendix, see "HYPAC User's Guide", B. Grundfelt, et al, Kemakta Report AR 89-18, Kemakta Consultants Co., Stockholm, Sweden, 1989.

Contents :

MESH GENERATION	A1
GENERAL PROPERTY ASSIGNEMENT	A1
CASE FIXZ1 - X36	A2
Property assignement	A2
Nammu & Post	A2
CASE FIXZ1A - X36FR	A3
Property assignement	A3
Nammu & Post	A3
CASE F1V1 - X36V1	A4
Property assignement	A4
Nammu & Post	A4
CASE F1V2 - X36V2	A5
Property assignement	A5
Nammu & Post	A5
CASE F1V3 - X36V3	A6
Mesh generation	A6
Property assignement	A6
Nammu & Post	A7
CASE F1V4 - X36V4	A8
Property assignement	A8
Nammu & Post	A8
CASE F1V8 - X36RM	A8
Property assignement	A8
Nammu & Post	A9
CASE F1V9 - X36IM	A10
Property assignement	A10
Nammu & Post	A10

MESH GENERATION

PFG : (Before PFG was run EMC was run. No errors or duplicate nodes where found.)

Input mesh file	=	pre/fixza.neu *
Output mesh file	=	pre/fixza.PFG
Output code file	=	pre/fixza.PFC
Shell script	=	pre/dopfg1 *

Repeated using pre/dopfg1 for :

Input mesh file	=	pre/fixzb.neu *
Input mesh file	=	pre/fixzc.neu *
Input mesh file	=	pre/fixzd.neu *
Input mesh file	=	pre/fixze.neu *
Input mesh file	=	pre/fixzf.neu *
Input mesh file	=	pre/fixzg.neu *
Input mesh file	=	pre/fixzh.neu *
Input mesh file	=	pre/fixzi.neu *
Input mesh file	=	pre/fixzj.neu *
Input mesh file	=	pre/fixzk.neu *
Input mesh file	=	pre/fixzl.neu *
Input mesh file	=	pre/fixzm.neu *
Input mesh file	=	pre/fixzn.neu *
Input mesh file	=	pre/fixzo.neu *

The script file pre/dopfg1 takes one argument
\$1 the letter (a-o) of the current mesh-file.

JTM : (The final mesh consisted of 18360 elements and 20720 nodes.)

Input mesh1 file	=	pre/fixza.PFG
Input code1 file	=	pre/fixza.PFC
Input mesh2 file	=	pre/fixzb.PFG
Input code2 file	=	pre/fixzb.PFC
Output mesh file	=	pre/fixzab.JTG
Output code file	=	pre/fixzab.JTC
Shell script	=	pre/dojtm1a *

Repeated for mesh parts c - o using pre/dojtm1 * resulting in the final mesh and code file :

Output mesh file	=	pre/fixzao.JTG
Output code file	=	pre/fixzao.JTC

The script file pre/dojtm1 takes two arguments where \$1 the letter (b-n) of the previous join and \$2 is the letter (c-o) of the current join.

OPT : (Front width was reduced to 896)

Input mesh file	=	pre/fixzao.JTG
Input code file	=	pre/fixzao.JTC
Output mesh file	=	pre/fixz1.OPG *
Output code file	=	pre/fixz1.OPC *
Shell script	=	pre/doopt1 *

GENERAL PROPERTY ASSIGNMENT

AMT :

Input mesh file	=	pre/fixz1.OPG
Input topog file	=	pre/fis.ssf *
Output mesh file	=	pre/fixz1.AMG
Shell script	=	pre/doamt1 *

BCA :

Input mesh file	=	pre/fixz1.AMG
Input code file	=	pre/fixz1.OPC
Output mesh file	=	pre/fixz1.BCG
Shell script	=	pre/dobcal *

PEA :

Input mesh file	=	pre/fixz1.BCG
Input code file	=	pre/fixz1.OPC
Output mesh file	=	pre/fixz1.PEG *
Shell script	=	pre/dopeal *

CASE FIXZ1 - X36

PROPERTY ASSIGNMENT

IFZ : The set of ifz runs was performed using the shell script pre/doifzf1 *

Input mesh file	=	pre/fixz1.PEG
Input code file	=	pre/fixz1.OPC
Input frac file	=	pre/fixz1.frc *
Output mesh file	=	pre/fixzf11.IFG
Output perm file	=	pre/fixzf11.IFP
Shell script	=	pre/doifzf1.1 *
Input mesh file	=	pre/fixzf11.IFG
Input perm file	=	pre/fixzf11.IFP
Input code file	=	pre/fixz1.OPC
Input frac file	=	pre/fixz1.frc
Output code file	=	pre/fixzf12.IFG
Output perm file	=	pre/fixzf12.IFP
Shell script	=	pre/doifzf1.2 *

The above step was repeated for fractures no. 3 - 19 resulting in :

Output code file	=	pre/fixzf119.IFG *
Output perm file	=	pre/fixzf119.IFP *

The script file pre/doifzf1.2 takes two arguments where \$1 the number (1-18) of the previous fracture assigned and \$2 is the number (2-19) of the current fracture.

NAMMU AND POSTPROCESSING

NAMMU :

Input mesh file	=	pre/fixzf119.IFG
Input perm file	=	pre/fixzf119.IFP
Input nam file	=	nammu/fixzf1.nam *
Output res file	=	nammu/fixzf1.res *
Shell script	=	nammu/donamf1 *

TRG :

Input mesh file	=	pre/fixzf119.IFG
Input perm file	=	pre/fixzf119.IFP
Input res file	=	nammu/fixzf1.res
Pathlines :		
Shell script	=	post1/doban1 *
Output path file(s)	=	post1/f1banB[1-8].DAT
Output path stat	=	post1/f1ban.LBN
Horizontal flux projection :		
Shell script	=	post1/dotrgf1 *
Output flux file	=	post1/f1f.DAT
Flux frequency :		
Shell script	=	post1/dofpr1 *
Output freq file	=	post1/f1fq.DAT
Vertical head projection :		
Shell script	=	post1/dotrgv1 *
Output head file	=	post1/f1v.GRD

CASE FIXZ1A - X36FR

PROPERTY ASSIGNMENT

IFZ : The set of ifz runs was performed using the shell script pre/doifzfla *

Input mesh file	=	pre/fixz1.PEG
Input code file	=	pre/fixz1.OPC
Input frac file	=	pre/fixz1a.frc *
Output mesh file	=	pre/fixzfla1.IFG
Output perm file	=	pre/fixzfla1.IFP
Shell script	=	pre/doifzfla.1 *
Input mesh file	=	pre/fixzfla1.IFG
Input perm file	=	pre/fixzfla1.IFP
Input code file	=	pre/fixz1.OPC
Input frac file	=	pre/fixz1a.frc
Output code file	=	pre/fixzfla2.IFG
Output perm file	=	pre/fixzfla2.IFP
Shell script	=	pre/doifzfla.2 *

The above step was repeated for fractures no. 3 - 19 resulting in :

Output code file	=	pre/fixzfla19.IFG *
Output perm file	=	pre/fixzfla19.IFP *

The script file pre/doifzfla.2 takes two arguments where \$1 the number (1-18) of the previous fracture assigned and \$2 is the number (2-19) of the current fracture.

NAMMU AND POSTPROCESSING

NAMMU :

Input mesh file	=	pre/fixzfla19.IFG
Input perm file	=	pre/fixzfla19.IFP
Input nam file	=	nammu/fixzfla.nam *
Output res file	=	nammu/fixzfla.res *
Shell script	=	nammu/donamfla *

TRG :

Input mesh file	=	pre/fixzfla19.IFG
Input perm file	=	pre/fixzfla19.IFP
Input res file	=	nammu/fixzfla.res
Pathlines :		
Shell script	=	post1/doban1a *
Output path file(s)	=	post1/flabanB[1-8].DAT
Output path stat	=	post1/flaban.LBN
Horizontal flux projection :		
Shell script	=	post1/dotrgfla *
Output flux file	=	post1/flaf.DAT
Flux frequency :		
Shell script	=	post1/dofpr1a *
Output freq file	=	post1/flafq.DAT
Vertical head projection :		
Shell script	=	post1/dotrgv1a *
Output head file	=	post1/flav.GRD

CASE F1V1 - X36V1

PROPERTY ASSIGNMENT

IFZ : The set of ifz runs was performed using the shell-script prev/doifzf1v1 * this script uses the scripts prev/doifzf1v1.1 * and prev/doifzf1v1.2 *

Table with 3 columns: File type, separator, and filename. It lists input and output files for two different stages of the process.

The above step was repeated for fractures no. 3,5-19 resulting in :

Table with 3 columns: File type, separator, and filename. It lists output files for fractures 3, 5-19.

The script-file doifzf1.2 takes two arguments where \$1 is the number (1-18) of the previous fracture assigned and \$2 is the number (2-19) of the current fracture.

The following permeability difference files were created during the process : prev/f1v110.IFH *, prev/f1v111.IFH *, prev/f1v112.IFH *, prev/f1v113.IFH *, prev/f1v114.IFH *, prev/f1v115.IFH *, prev/f1v116.IFH *, prev/f1v117.IFH *, prev/f1v118.IFH *, prev/f1v119.IFH *, prev/f1v12.IFH *, prev/f1v13.IFH *, prev/f1v15.IFH *, prev/f1v16.IFH *, prev/f1v17.IFH *, prev/f1v18.IFH * and prev/f1v19.IFH *

NAMMU AND POSTPROCESSING

NAMMU:

Table with 3 columns: File type, separator, and filename. It lists input and output files for the NAMMU process.

TRG

Table with 3 columns: File type, separator, and filename. It lists input and output files for the TRG process, including pathlines, horizontal flux projection, and vertical head projection.

CASE F1V2 - X36V2

PROPERTY ASSIGNEMENT

*IFZ: The ifz run was performed using the shell-script prev/doifzf1v2 **

Input mesh file	=	pre/fixz1.PEG
Input code file	=	pre/fixz1.OPC
Input frac file	=	prev/f1v2.frc *
Shell script	=	prev/doifzf1v2 *
Output mesh file	=	prev/f1v24.IFG
Output perm file	=	prev/f1v24.IFP
Output pdiff file	=	prev/f1v24.IFH *

*JIF: The jif run was performed using the shell-script prev/dojiff1v2 **

Input mesh file	=	prev/f1v24.IFG
Input perm file	=	prev/f1v11.IFP
Input pdiff file	=	prev/f1v24.IFH
Input pdiff file	=	prev/f1v1[2-3,5-19].IFH
Shell script	=	prev/dojiff1v2 *
Output perm file	=	prev/f1v24.JIP *

NAMMU AND POSTPROCESSING

NAMMU:

Input mesh file	=	prev/f1v24.IFG
Input perm file	=	prev/f1v24.JIP
Input nam file	=	nammu/f1v2.nam *
Input script-file	=	nammu/donamf1v2 *
Output res file	=	nammu/f1v2.res * (unformatted)
Output res file	=	nammu/f1v2.RES * (formatted)

TRG :

Input mesh file	=	prev/f1v24.IFG
Input perm file	=	prev/f1v24.JIP
Input res file	=	nammu/f1v2.RES
Pathlines :		
Shell script	=	post1v2/doban1v2 *
Output path file(s)	=	post1v2/f1v2bB[1-8].DAT
Output path stat	=	post1v2/f1v2b.LBN
Horizontal flux projection :		
Shell script	=	post1v2/dotrgf1v2 *
Output flux file	=	post1v2/f1v2f.DAT
Flux frequency :		
Shell script	=	post1v2/dofpr1v2 *
Output freq file	=	post1v2/f1v2fq.DAT
Vertical head projection :		
Shell script	=	post1v2/dotrgv1v2 *
Output head file	=	post1v2/f1v2v.GRD

CASE F1V3 - X36V3

MESH GENERATION

PFG: (Before PFG was run EMC was run. No errors or duplicate nodes where found.)

Input mesh file	=	prev3/fixzkkx.neu *
Output mesh file	=	prev3/fixz1v3kk.PFG
Output code file	=	prev3/fixz1v3kk.PFC
Shell script	=	prev3/dopfg1v3 *

Repeated using prev3/dopfg1v3 for :

Input mesh file	=	prev3/fixzlx.neu *
Input mesh file	=	prev3/fixzmx.neu *

The script file prev3/dopfg1v3 takes one argument
\$1 the letter (kx-mx) of the current mesh-file.

JTM: (The final mesh consisted of 25704 elements and 28490 nodes.)

Input mesh1 file	=	pre/fixzaj.PFG
Input code1 file	=	pre/fixzaj.PFC
Input mesh2 file	=	prev3/fixz1v3kk.PFG
Input code2 file	=	prev3/fixz1v3kk.PFC
Output mesh file	=	prev3/fixz1v3akx.JTG
Output code file	=	prev3/fixz1v3akx.JTC
Shell script	=	prev3/dojtm1v3a *

Repeated for mesh parts lx,mx,n - o using prev3/dojtm1v3 * resulting
in the final mesh and code file :

Output mesh file	=	prev3/fixz1v3ao.JTG
Output code file	=	prev3/fixz1v3ao.JTC

The script file prev3/dojtm1v3 takes two arguments where
\$1 the letter (j,kx-mx) of the previous join and \$2 is the letter
(kx-o) of the current join.

OPT: (Final front width 1232.)

Input mesh file	=	prev3/fixz1v3ao.JTG
Input code file	=	prev3/fixz1v3ao.JTC
Output mesh file	=	prev3/fixz1v3.OPG *
Output code file	=	prev3/fixz1v3.OPC *
Shell script	=	prev3/doopt1v3 *

PROPERTY ASSIGNEMENT

AMT:

Input mesh file	=	prev3/fixz1v3.OPG
Input topog file	=	pre/fis.ssf *
Output mesh file	=	prev3/fixz1v3.AMG
Shell script	=	prev3/doamt1v3 *

BCA:

Input mesh file	=	prev3/fixz1v3.AMG
Input code file	=	prev3/fixz1v3.OPC
Output mesh file	=	prev3/fixz1v3.BCG
Shell script	=	prev3/dobca1v3 *

PEA:

Input mesh file	=	prev3/fixz1v3.BCG
Input code file	=	prev3/fixz1v3.OPC
Output mesh file	=	prev3/fixz1v3.PEG *
Shell script	=	prev3/dopea1v3 *

*IFZ: The set of ifz runs was performed using the shell-script prev/doifzf1v3 * this script uses the scripts prev/doifzf1v3.1 * and prev/doifzf1v3.2 **

```

Input mesh file           =           prev3/fixz1v3.PEG
Input code file           =           prev3/fixz1v3.OPC
Input frac file           =           prev3/f1v3.frc *
Shell script              =           prev3/doi1zf1v3.1 *
Output mesh file          =           prev3/f1v31.IFG
Output perm file          =           prev3/f1v31.IFP
Output pdiff file         =           prev3/f1v31.IFH *

Input mesh file           =           prev3/f1v31.IFG
Input perm file           =           prev3/f1v31.IFP
Input code file           =           prev3/fixz1v3.OPC
Input frac file           =           prev3/f1v3.frc
Shell script              =           prev3/doi1zf1v3.2 *
Output mesh file          =           prev3/f1v32.IFG
Output perm file          =           prev3/f1v32.IFP
Output pdiff file         =           prev3/f1v32.IFH

```

The above step was repeated for fractures no. 3-20 resulting in :

```

Output mesh file          =           prev3/f1v320.IFG *
Output perm file          =           prev3/f1v320.IFP *
Output pdiff file         =           prev3/f1v320.IFH *

```

The script-file doi1zf1.2 takes two arguments where \$1 is the number (1-19) of the previous fracture assigned and \$2 is the number (2-20) of the current fracture.

The following permeability difference files were created during the process :

prev3/f1v310.IFH *, prev3/f1v311.IFH *, prev3/f1v312.IFH *, prev3/f1v313.IFH *, prev3/f1v314.IFH *, prev3/f1v315.IFH *, prev3/f1v316.IFH *, prev3/f1v317.IFH *, prev3/f1v318.IFH *, prev3/f1v319.IFH *, prev3/f1v32.IFH *, prev3/f1v33.IFH *, prev3/f1v35.IFH *, prev3/f1v36.IFH *, prev3/f1v37.IFH *, prev3/f1v38.IFH *, prev3/f1v320.IFH * and prev3/f1v39.IFH *

NAMMU AND POSTPROCESSING

NAMMU:

```

Input mesh file           =           prev3/f1v320.IFG
Input perm file           =           prev3/f1v320.IFP
Input nam file            =           nammu/f1v3.nam *
Input script-file         =           nammu/donamf1v3 *
Output res file           =           nammu/f1v3.res * (unformatted)
Output res file           =           nammu/f1v3.RES * (formatted)

```

TRG :

```

Input mesh file           =           prev3/f1v320.IFG
Input perm file           =           prev3/f1v320.IFP
Input res file            =           nammu/f1v3.RES

Pathlines :
Shell script              =           post1v3/doban1v3 *
Output path file(s)       =           post1v3/f1v3b[1-8].DAT
Output path stat          =           post1v3/f1v3b.LBN

Horizontal flux projection :
Shell script              =           post1v3/dotrgf1v3 *
Output flux file          =           post1v3/f1v3f.DAT

Flux frequency :
Shell script              =           post1v3/dofpr1v3 *
Output freq file          =           post1v3/f1v3fq.DAT

Vertical head projection :
Shell script              =           post1v3/dotrgv1v3 *
Output head file          =           post1v3/f1v3v.GRD

```

CASE F1V4 - X36V4

PROPERTY ASSIGNEMENT

JIF: The jif run was performed using the shell-script prev3/dojiff1v4 *

Input mesh file	=	prev3/f1v31.IFG
Input perm file	=	prev3/f1v31.IFP
Input pdiff file	=	prev3/f1v1[2-3,5-20].IFH
Shell script	=	prev3/dojiff1v4 *
Output perm file	=	prev3/f1v41.JIP *

NAMMU AND POSTPROCESSING

NAMMU:

Input mesh file	=	prev3/f1v320.IFG
Input perm file	=	prev3/f1v41.JIP
Input nam file	=	nammu/f1v4.nam *
Input script-file	=	nammu/donamf1v4 *
Output res file	=	nammu/f1v4.res * (unformatted)
Output res file	=	nammu/f1v4.RES * (formatted)

TRG

Input mesh file	=	prev3/f1v320.IFG
Input perm file	=	prev3/f1v41.JIP
Input res file	=	nammu/f1v4.RES
Pathlines :		
Shell script	=	post1v4/doban1v4 *
Output path file(s)	=	post1v4/f1v4bB[1-8].DAT
Output path stat	=	post1v4/f1v4b.LBN
Horizontal flux projection :		
Shell script	=	post1v4/dotrgf1v4 *
Output flux file	=	post1v4/f1v4f.DAT
Flux frequency :		
Shell script	=	post1v4/dofpr1v4 *
Output freq file	=	post1v4/f1v4fq.DAT
Vertical head projection :		
Shell script	=	post1v4/dotrgv1v4 *
Output head file	=	post1v4/f1v4v.GRD

CASE F1V8 - X36RM

PROPERTY ASSIGNEMENT

PEA :

Input mesh file	=	pre/fixz1.BCG
Input code file	=	pre/fixz1.OPC
Output mesh file	=	pre/f1v8.PEG *
Output perm file	=	pre/f1v8.PEP *
Shell script	=	pre/dopeaf1v8 *

JIF: The jif run was performed using the shell-script preldojiff1v8.1 *

Input perm file	=	pre/f1v8.PEP
Input pdiff file	=	pre/f1v9[1-13].IFH
Shell script	=	pre/dojiff1v8.1 *
Output perm file	=	pre/f1v81.JIP *

IFZ: The set of ifz runs was performed using the shell-script *pre/doifzf1v8 **.

Input mesh file	=	pre/f1v8.PEG
Input perm file	=	pre/f1v81.JIP
Input code file	=	pre/fixz1.OPC
Input frac file	=	pre/f1v8.frc *
Shell script	=	pre/doifzf1v8 *
Output mesh file	=	pre/f1v814.IFG
Output perm file	=	pre/f1v814.IFP
Output pdiff file	=	pre/f1v814.IFH *
Input mesh file	=	pre/f1v814.IFG
Input perm file	=	pre/f1v814.IFP
Input code file	=	pre/fixz1.OPC
Input frac file	=	pre/f1v8.frc
Shell script	=	pre/doifzf1v8 *
Output mesh file	=	pre/f1v815.IFG
Output perm file	=	pre/f1v815.IFP
Output pdiff file	=	pre/f1v815.IFH

The script-file *doifzf1v8* takes two arguments where \$1 is the number (1-19) of the previous fracture assigned and \$2 is the number (2-20) of the current fracture.

JIF: The jif run was performed using the shell-script *pre/dojiff1v8.2 **

Input perm file	=	pre/f1v815.IFP
Input pdiff file	=	pre/f1v9[16-19].IFH
Shell script	=	pre/dojiff1v8.2 *
Output perm file	=	pre/f1v82.JIP *

NAMMU AND POSTPROCESSING

NAMMU:

Input mesh file	=	pre/f1v815.IFG
Input perm file	=	pre/f1v82.JIP
Input nam file	=	nammu/f1v8.nam *
Input script-file	=	nammu/donamf1v8 *
Output res file	=	nammu/f1v8.res * (unformatted)
Output res file	=	nammu/f1v8.RES * (formatted)

TRG

Input mesh file	=	pre/f1v815.IFG
Input perm file	=	pre/f1v82.JIP
Input res file	=	nammu/f1v8.RES
Pathlines :		
Shell script	=	post1v8/doban1v8 *
Output path file(s)	=	post1v8/f1v8bB[1-8].DAT
Output path stat	=	post1v8/f1v8b.LBN
Horizontal flux projection :		
Shell script	=	post1v8/dotrgf1v8 *
Output flux file	=	post1v8/f1v8f.DAT
Flux frequency :		
Shell script	=	post1v8/dofpr1v8 *
Output freq file	=	post1v8/f1v8fq.DAT
Vertical head projection :		
Shell script	=	post1v8/dotrgv1v8 *
Output head file	=	post1v8/f1v8v.GRD

CASE F1V9 - X36IM

PROPERTY ASSIGNEMENT

IFZ: The set of ifz runs was performed using the shell-script *pre/doifzf1v9* * this script uses the scripts *pre/doifzf1v9.1* * and *pre/doifzf1v9.2* *

Input mesh file	=	<i>pre/f1v9.PEG</i>
Input code file	=	<i>pre/f1v9.OPC</i>
Input frac file	=	<i>pre/f1v9.frc</i> *
Shell script	=	<i>pre/doifzf1v9.1</i> *
Output mesh file	=	<i>pre/f1v91.IFG</i>
Output perm file	=	<i>pre/f1v91.IFP</i>
Output pdiff file	=	<i>pre/f1v91.IFH</i> *
Input mesh file	=	<i>pre/f1v91.IFG</i>
Input perm file	=	<i>pre/f1v91.IFP</i>
Input code file	=	<i>pre/f1v9.OPC</i>
Input frac file	=	<i>pre/f1v9.frc</i>
Shell script	=	<i>pre/doifzf1v9.2</i> *
Output mesh file	=	<i>pre/f1v92.IFG</i>
Output perm file	=	<i>pre/f1v92.IFP</i>
Output pdiff file	=	<i>pre/f1v92.IFH</i>

The above step was repeated for fractures no. 3-19 resulting in :

Output mesh file	=	<i>pre/f1v919.IFG</i> *
Output perm file	=	<i>pre/f1v919.IFP</i> *
Output pdiff file	=	<i>pre/f1v919.IFH</i> *

The script-file *doifzf1.2* takes two arguments where \$1 is the number (1-18) of the previous fracture assigned and \$2 is the number (2-19) of the current fracture.

The following permeability difference files were created during the process :

pre/f1v910.IFH *, *pre/f1v911.IFH* *, *pre/f1v912.IFH* *, *pre/f1v913.IFH* *, *pre/f1v914.IFH* *, *pre/f1v915.IFH* *, *pre/f1v916.IFH* *, *pre/f1v917.IFH* *, *pre/f1v918.IFH* *, *pre/f1v919.IFH* *, *pre/f1v91.IFH* *, *pre/f1v92.IFH* *, *pre/f1v93.IFH* *, *pre/f1v95.IFH* *, *pre/f1v96.IFH* *, *pre/f1v97.IFH* *, *pre/f1v98.IFH* *, *pre/f1v920.IFH* * and *pre/f1v99.IFH* *

NAMMU AND POSTPROCESSING

NAMMU:

Input mesh file	=	<i>pre/f1v919.IFG</i>
Input perm file	=	<i>pre/f1v919.IFP</i>
Input nam file	=	<i>nammu/f1v9.nam</i> *
Input script-file	=	<i>nammu/donamf1v9</i> *
Output res file	=	<i>nammu/f1v9.res</i> * (unformatted)
Output res file	=	<i>nammu/f1v9.RES</i> * (formatted)

TRG

Input mesh file	=	<i>pre/f1v919.IFG</i>
Input perm file	=	<i>pre/f1v919.IFP</i>
Input res file	=	<i>nammu/f1v9.RES</i>
Pathlines :		
Shell script	=	<i>post1v9/doban1v9</i> *
Output path file(s)	=	<i>post1v9/f1v9bB[1-8].DAT</i>
Output path stat	=	<i>post1v9/f1v9b.LBN</i>
Horizontal flux projection :		
Shell script	=	<i>post1v9/dotrgf1v9</i> *
Output flux file	=	<i>post1v9/f1v9f.DAT</i>
Flux frequency :		
Shell script	=	<i>post1v9/dofpr1v9</i> *
Output freq file	=	<i>post1v9/f1v9fq.DAT</i>
Vertical head projection :		
Shell script	=	<i>post1v9/dotrgv1v9</i> *
Output head file	=	<i>post1v9/f1v9v.GRD</i>

Appendix B

Evaluation figures not presented in the current text

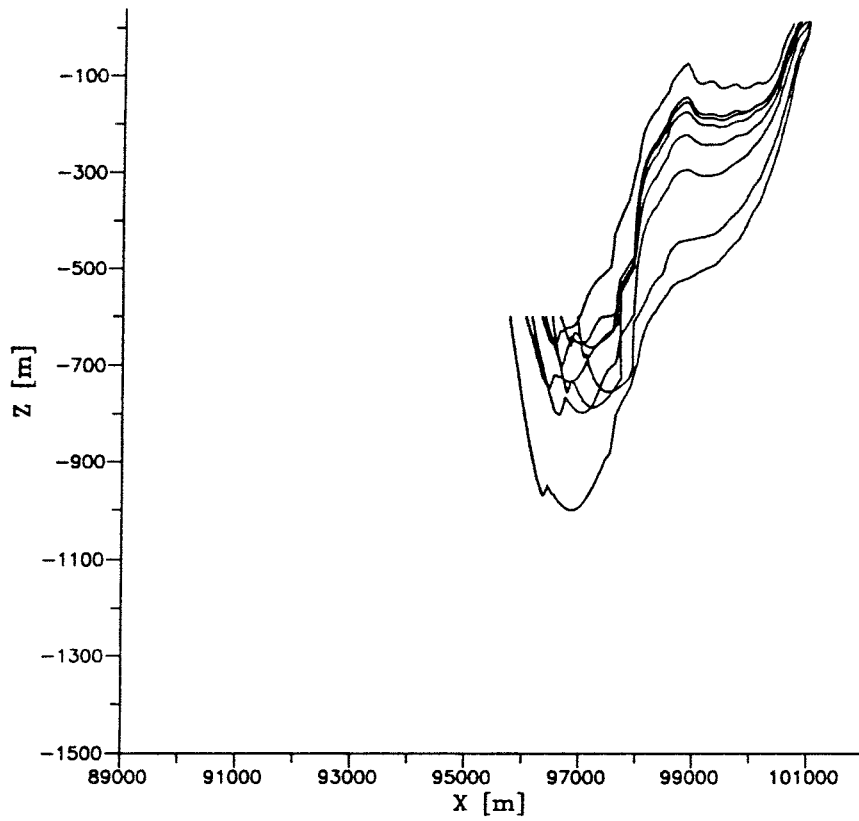


Figure B1 Vertical view of pathlines (xz-plane) for Case X36.

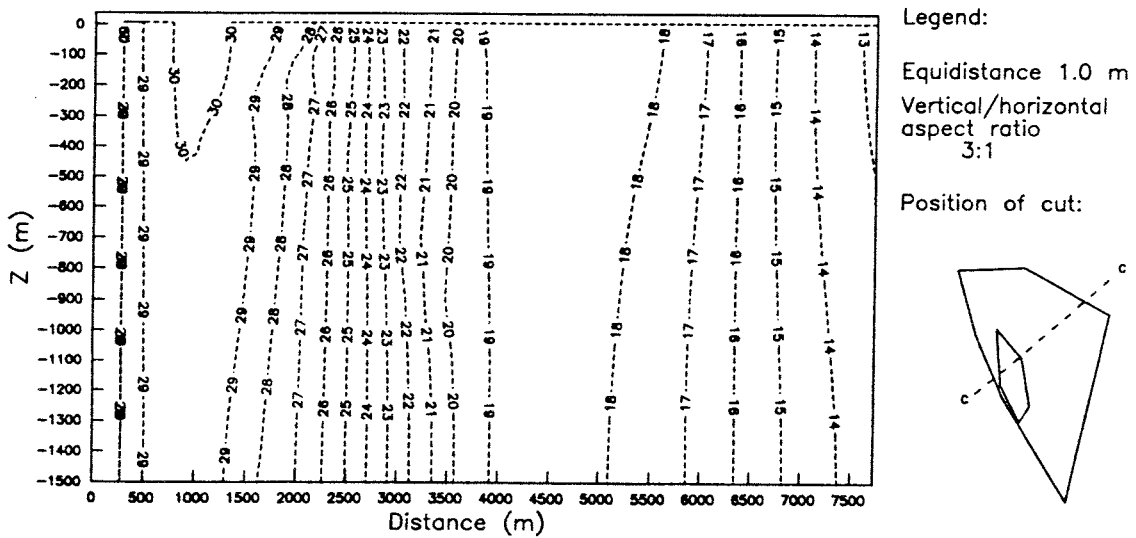


Figure B2 Distribution of hydraulic head in a vertical cut for Case X36FR.

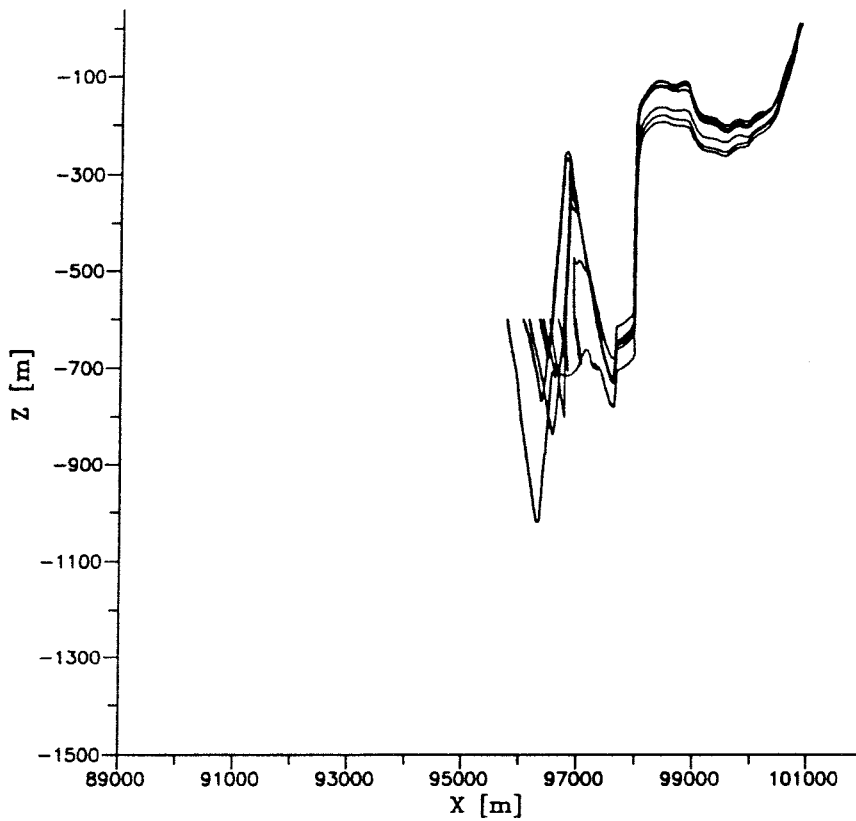


Figure B3 Vertical view of pathlines (xz-plane) for Case X36FR.

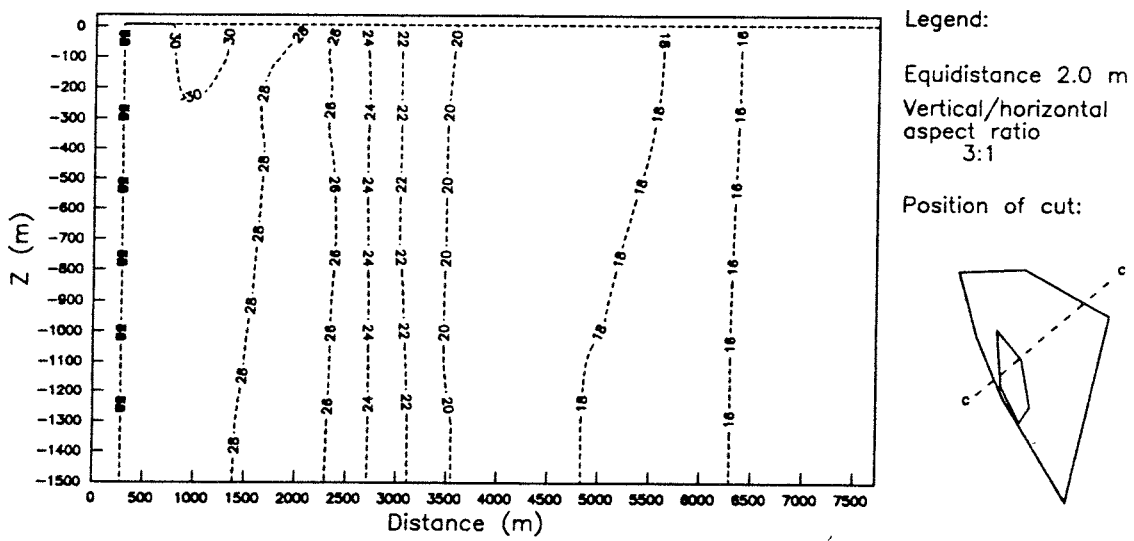


Figure B4 Distribution of hydraulic head in a vertical cross-section for Case X36RM.

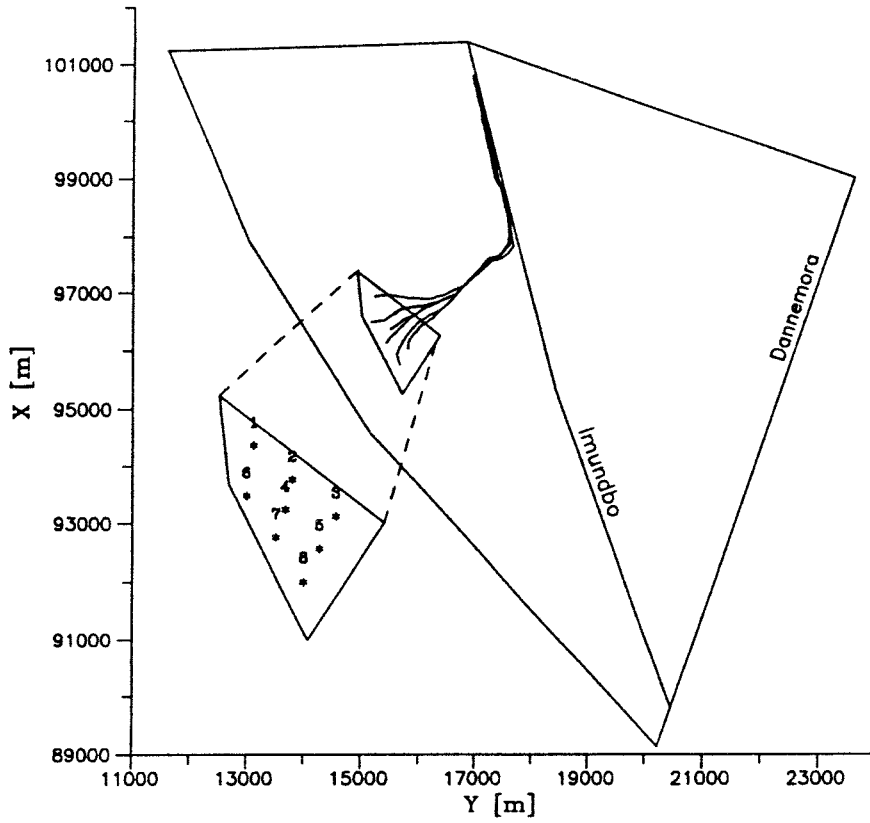


Figure B5 Horizontal projection of pathlines for Case X36RM.

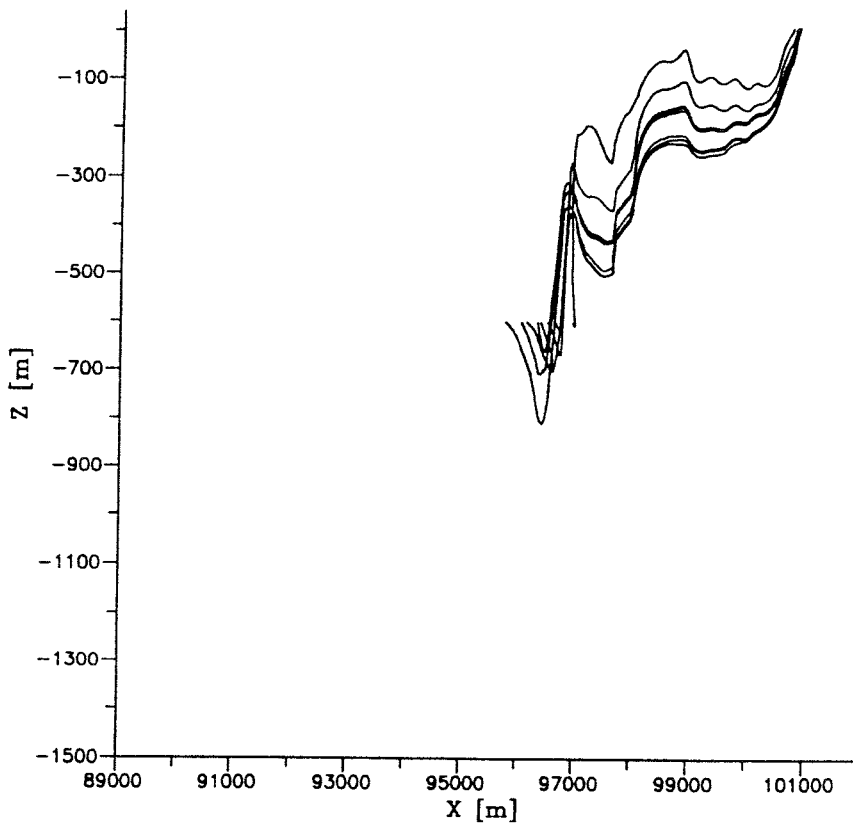


Figure B6 Vertical projection (xz-plane) of pathlines for Case X36RM.

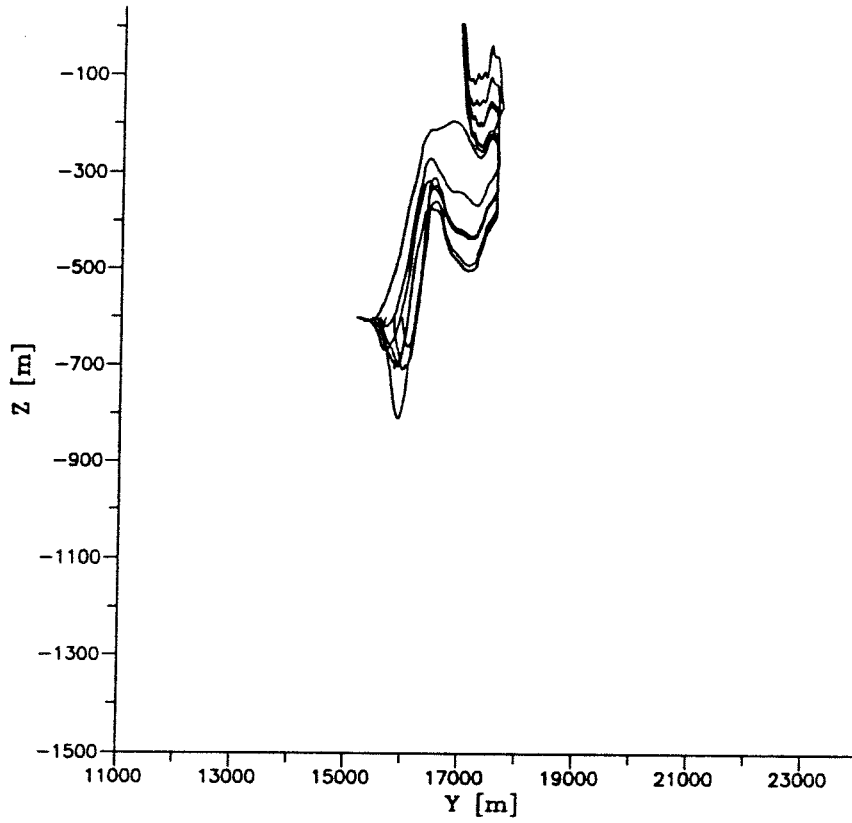


Figure B7 Vertical projection (yz-plane) of pathlines for Case X36RM.

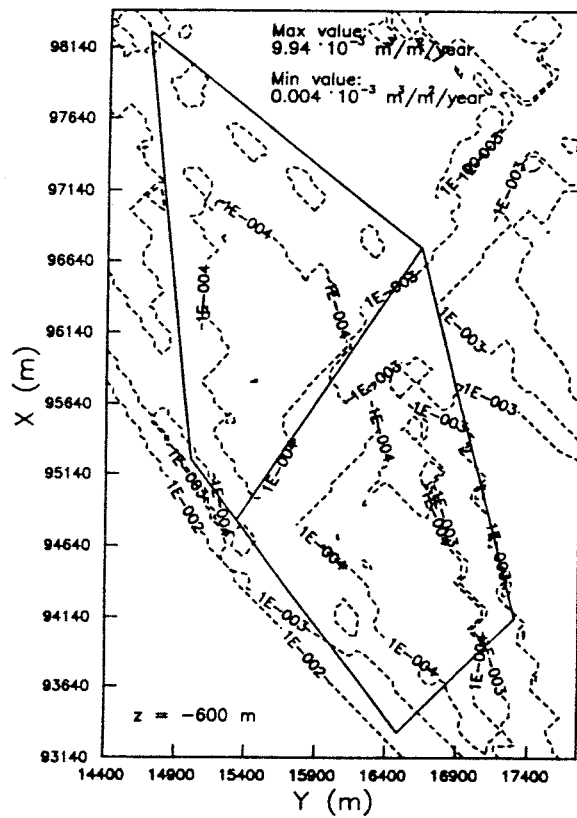


Figure B8 Contoured flux distribution ($\text{m}^3/\text{m}^2/\text{year}$) for Case X36RM.

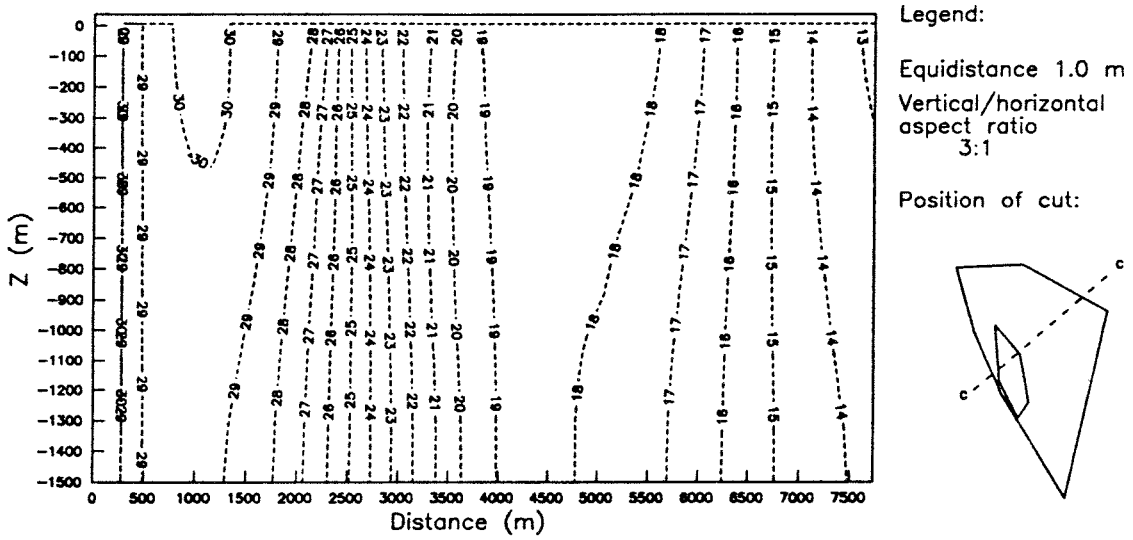


Figure B9 Distribution of hydraulic head in a vertical cross section for Case X36V1.

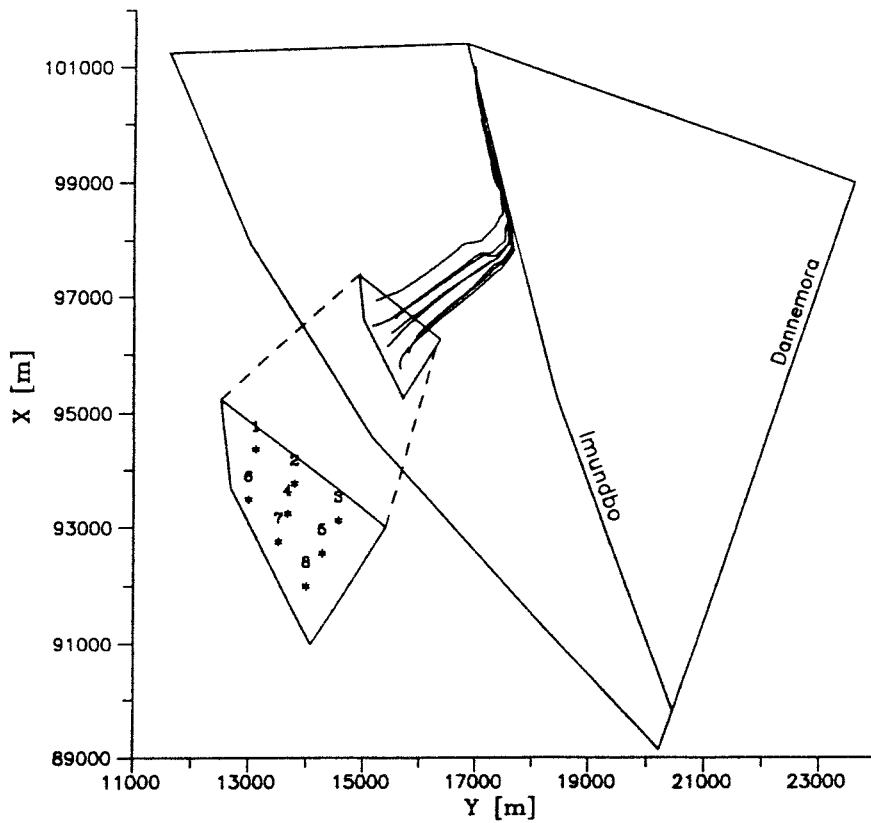


Figure B10 Horizontal view of pathlines for Case X36V1.

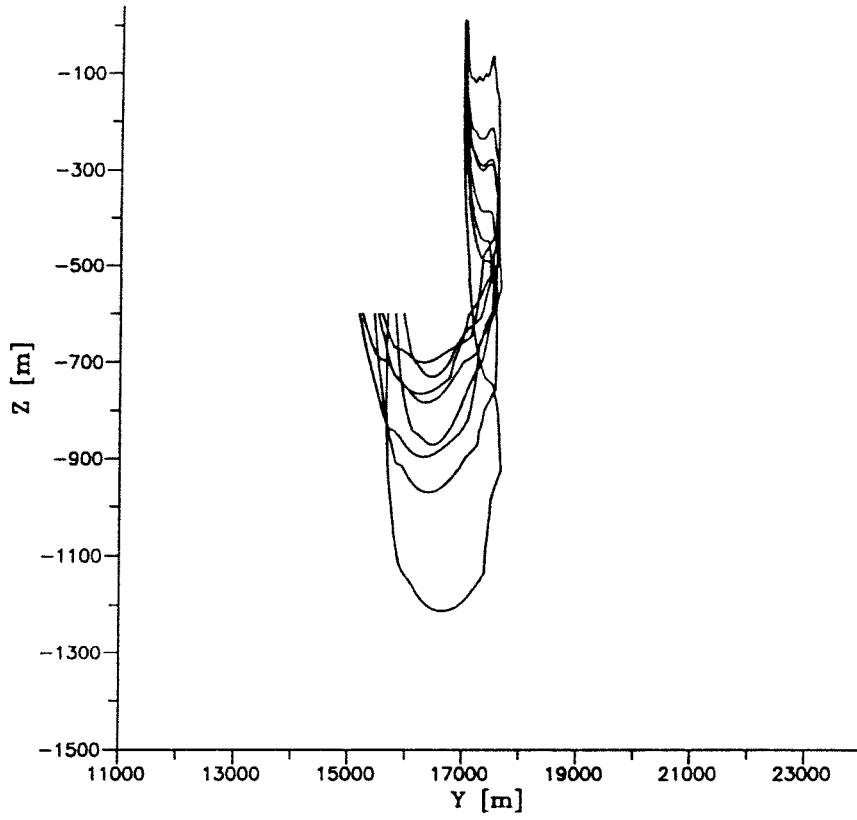


Figure B11 Vertical view of pathlines (yz-plane) for Case X36V1.

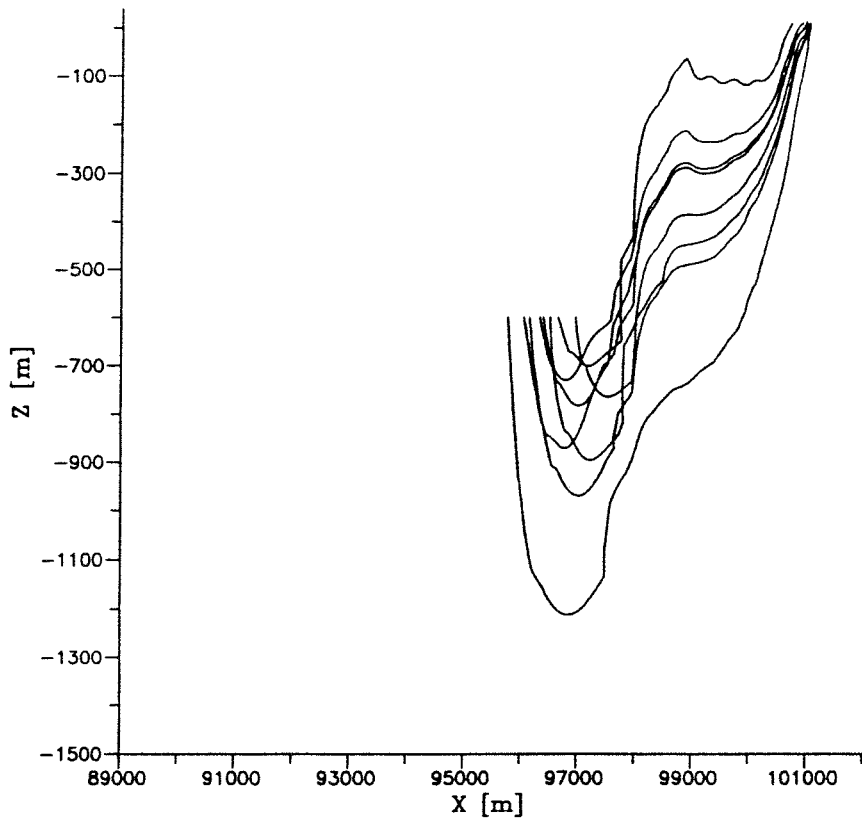


Figure B12 Vertical view (xz-plane) of pathlines for Case X36V1.

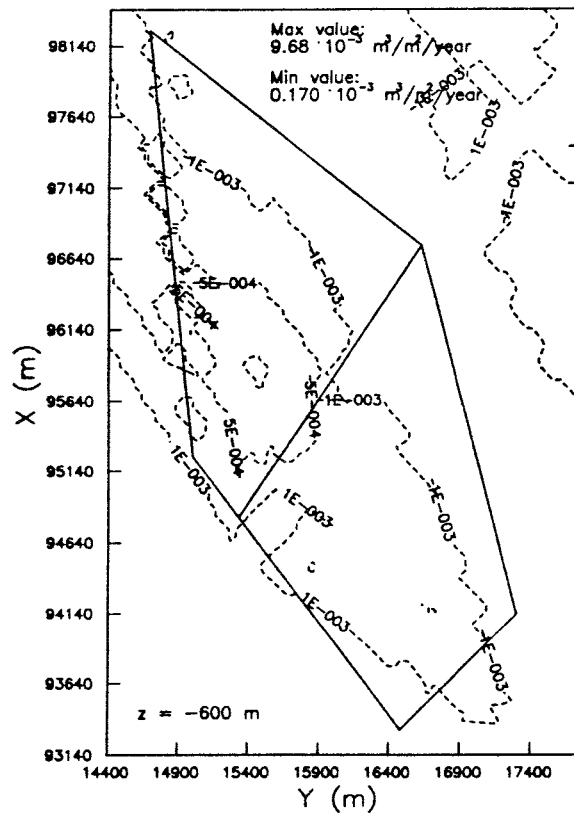


Figure B13 Contoured flux distribution ($\text{m}^3/\text{m}^2/\text{year}$) for Case X36V1.

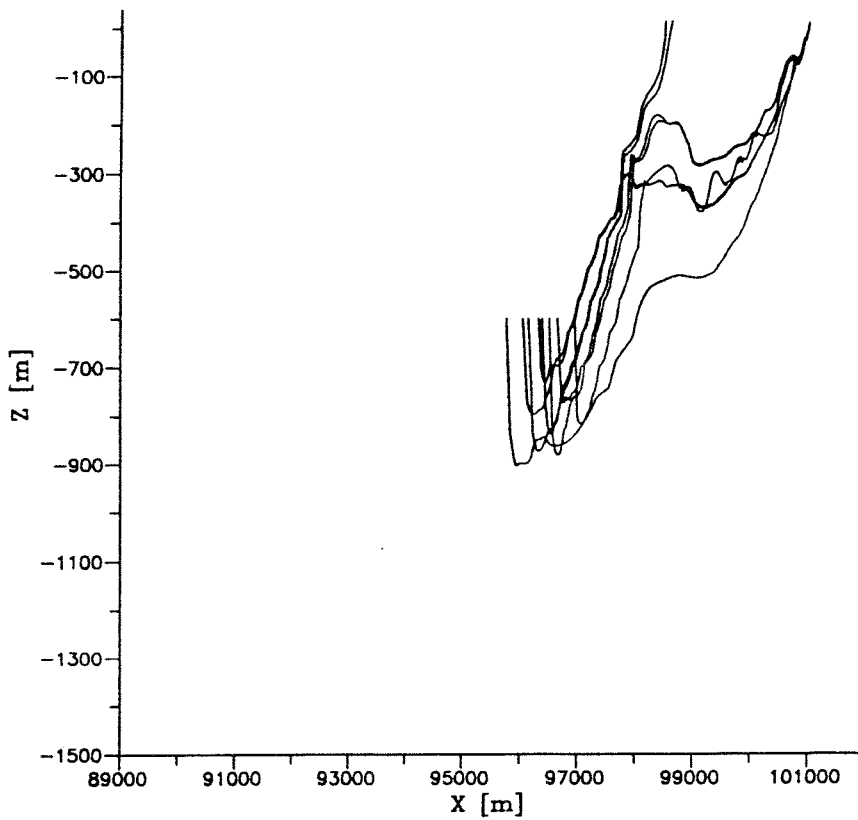


Figure B14 Vertical view (xz-plane) of pathlines for Case X36V3.

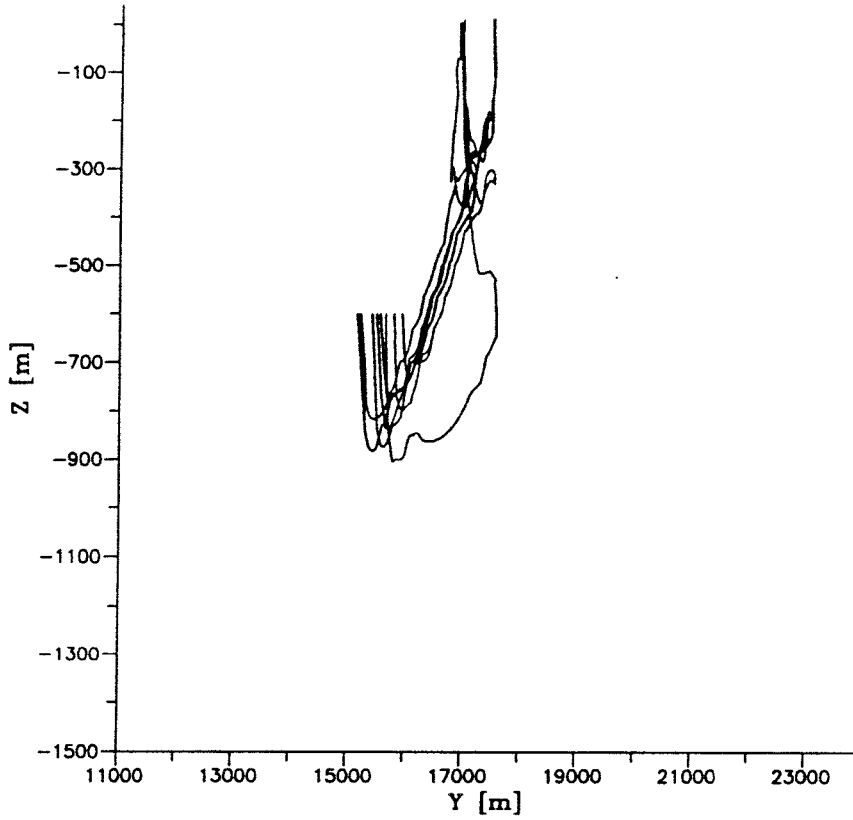


Figure B15 Vertical view (yz-plane) of pathlines for Case X36V3.

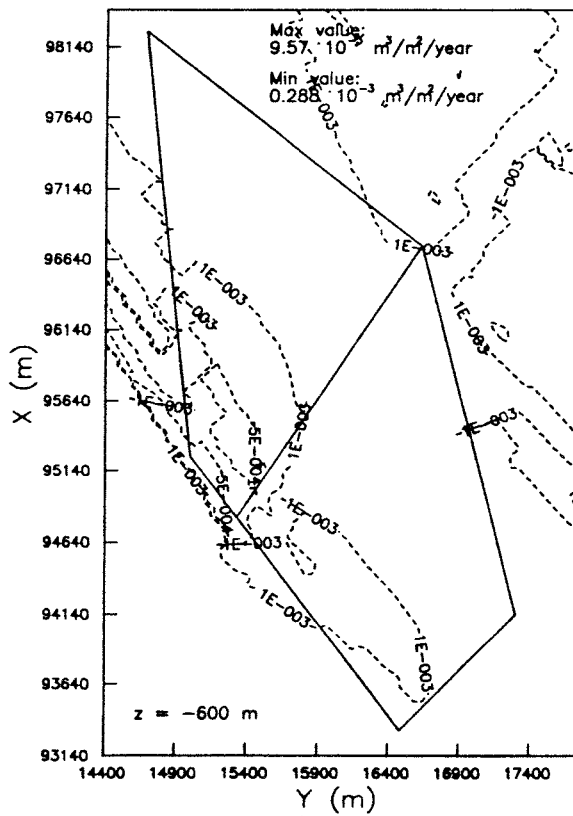


Figure B16 Contoured flux distribution ($m^3/m^2/year$) for Case X36V3.

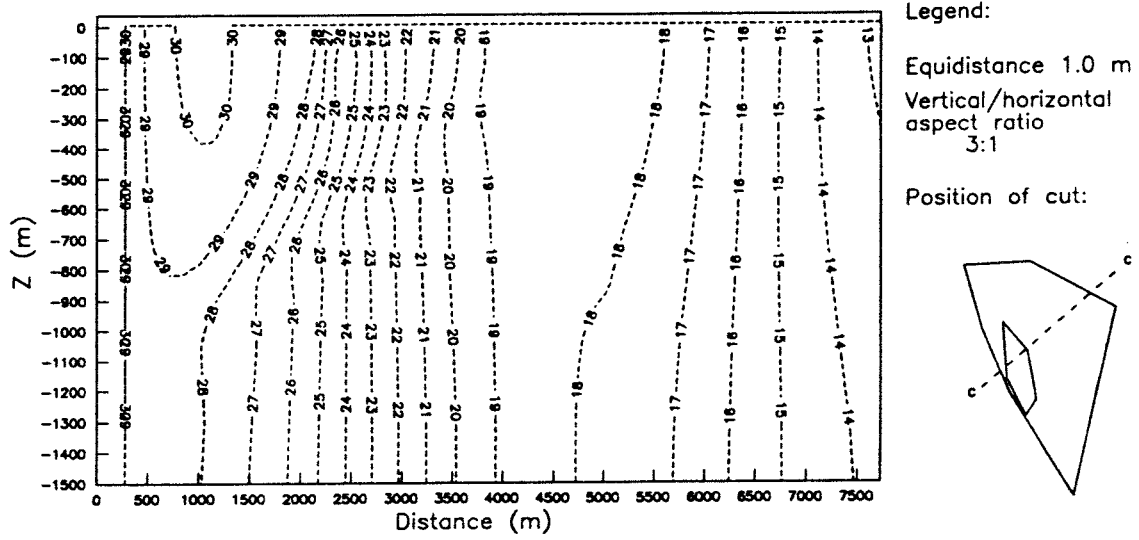


Figure B17 Distribution of hydraulic head in a vertical cross section for Case X36V4.

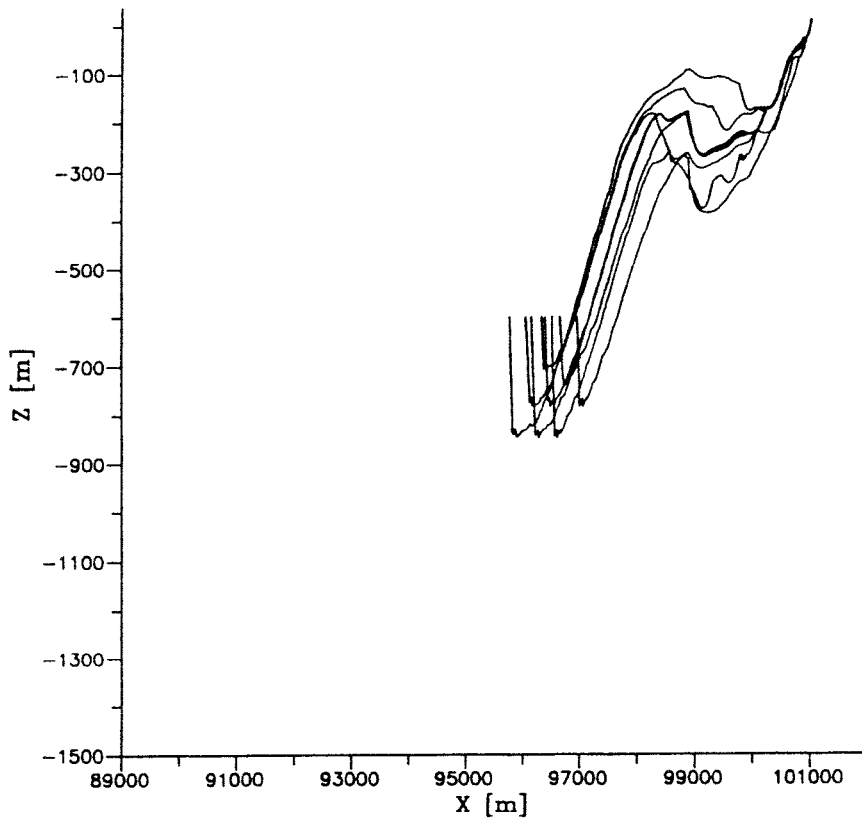


Figure B18 Vertical view (xz-plane) of pathlines for Case X36V4.

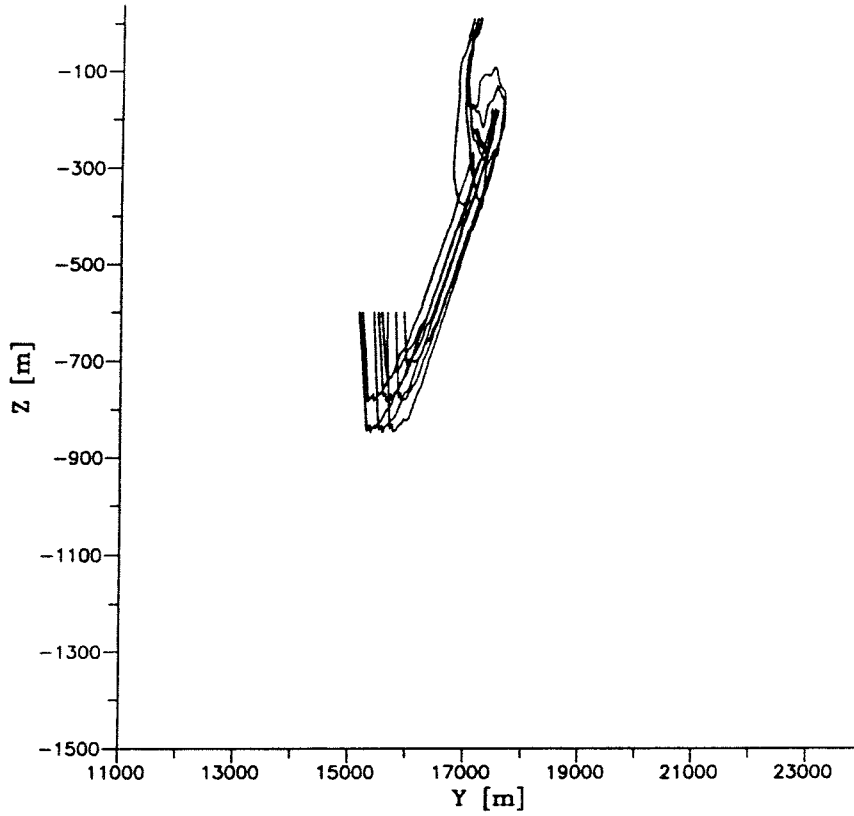


Figure B19 Vertical view (yz-plane) of pathlines for Case X36V4.

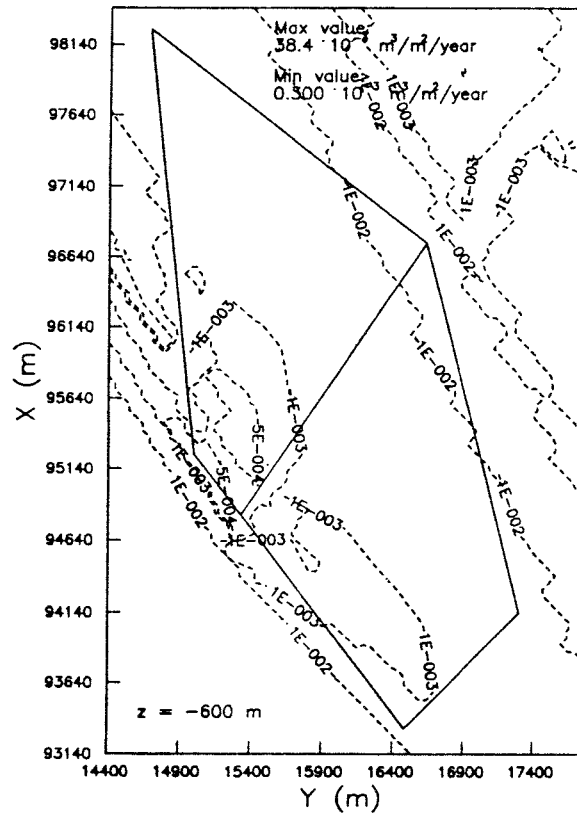


Figure B20 Contoured flux distribution ($\text{m}^3/\text{m}^2/\text{year}$) at repository level for Case X36V4.

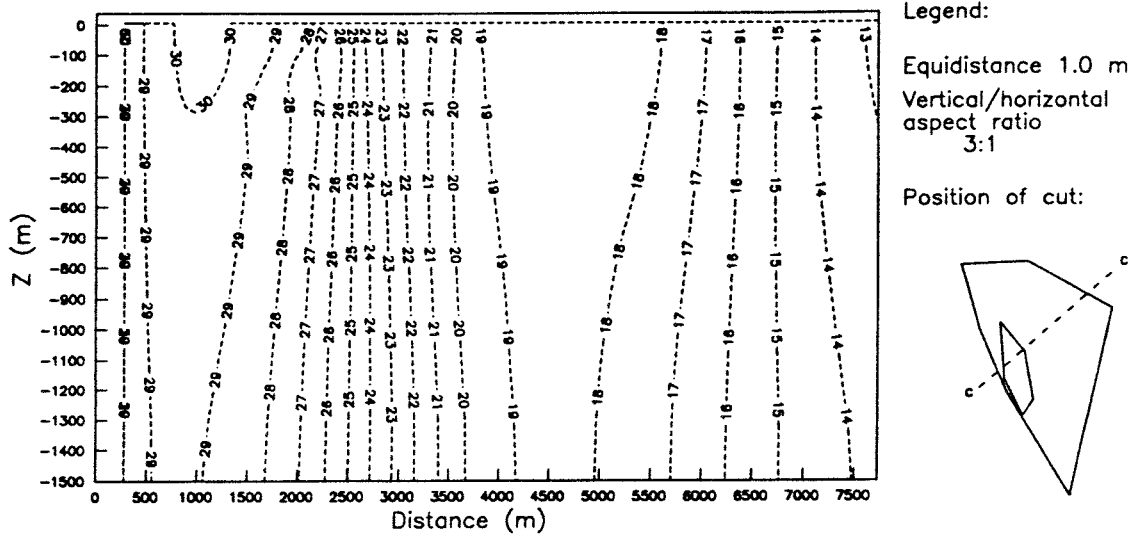


Figure B21 Distribution of hydraulic head in a vertical cross section for Case X36V2.

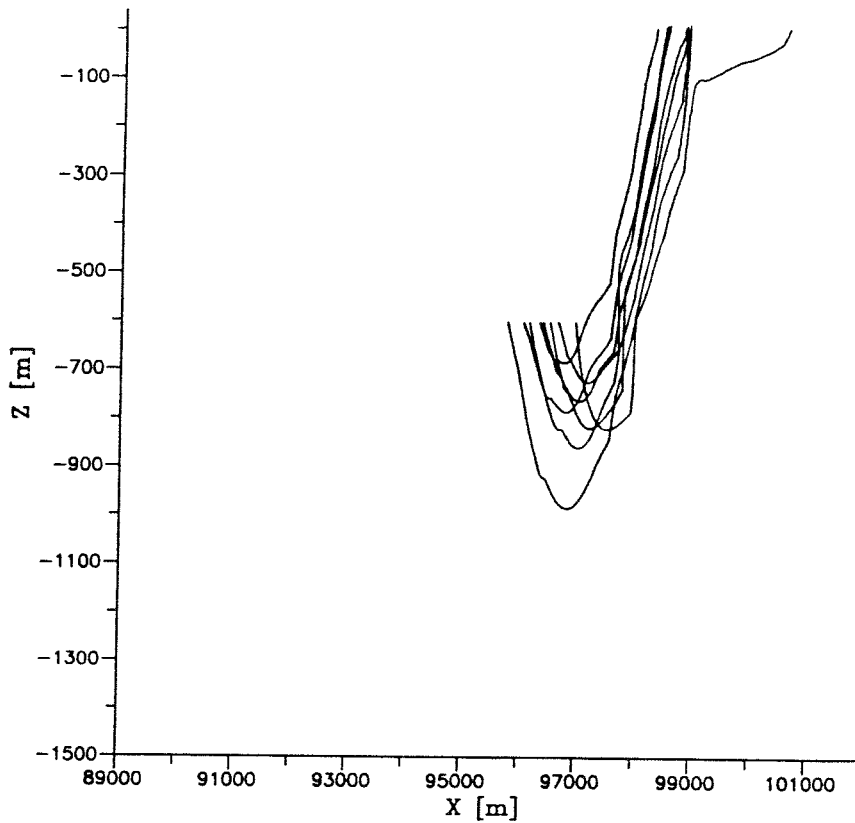


Figure B22 Vertical view (xz-plane) of pathlines for Case X36V2.

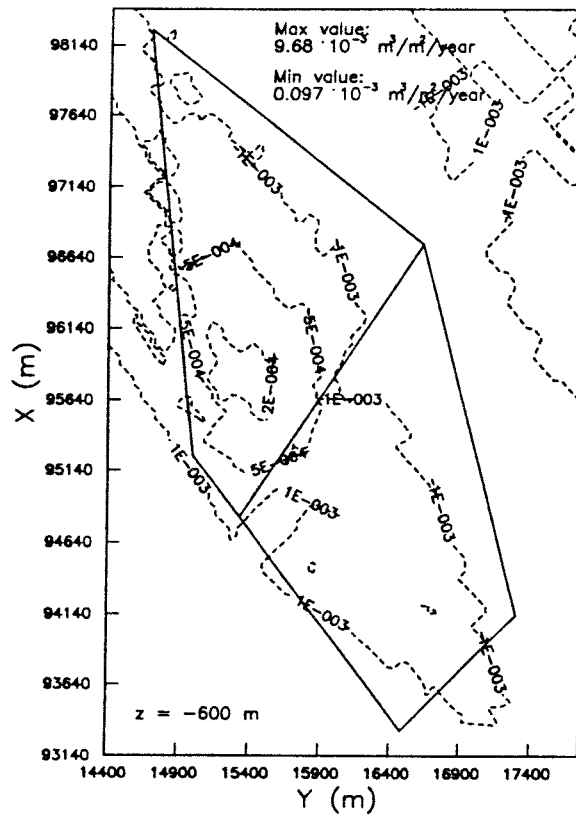


Figure B23 Contoured flux distribution ($m^3/m^2/year$) for Case X36V2.

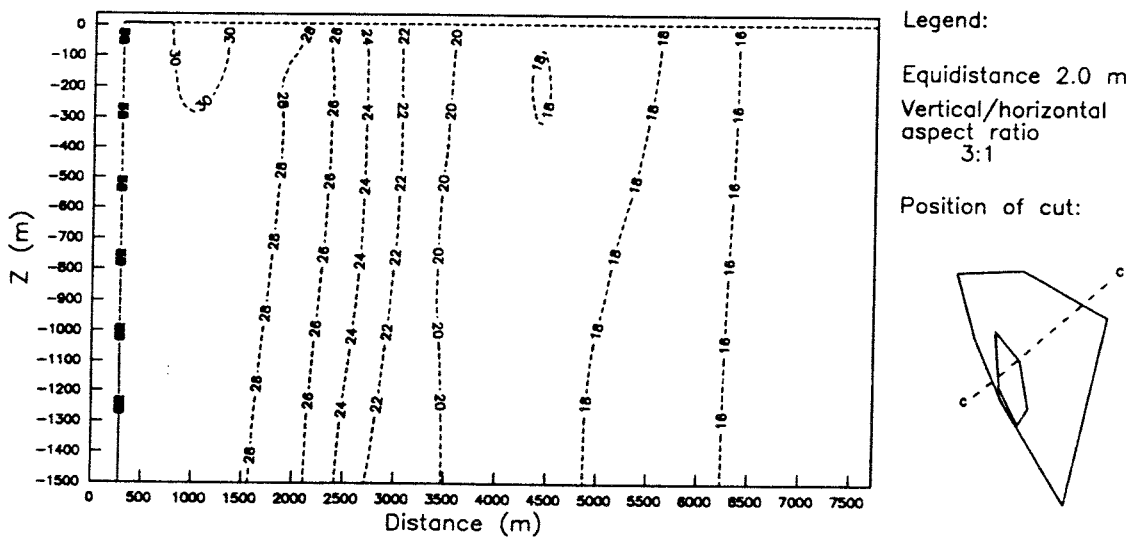


Figure B24 Distribution of hydraulic head in a vertical cross-section for Case X36IM.

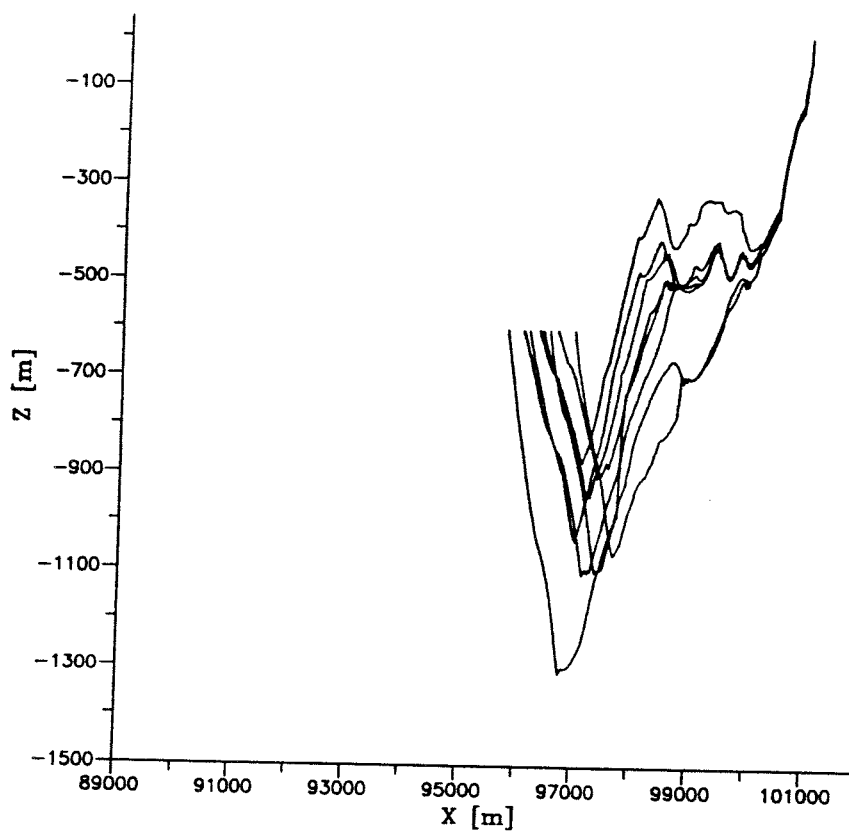


Figure B25 Vertical projection (xz-plane) of pathlines for Case X36IM.

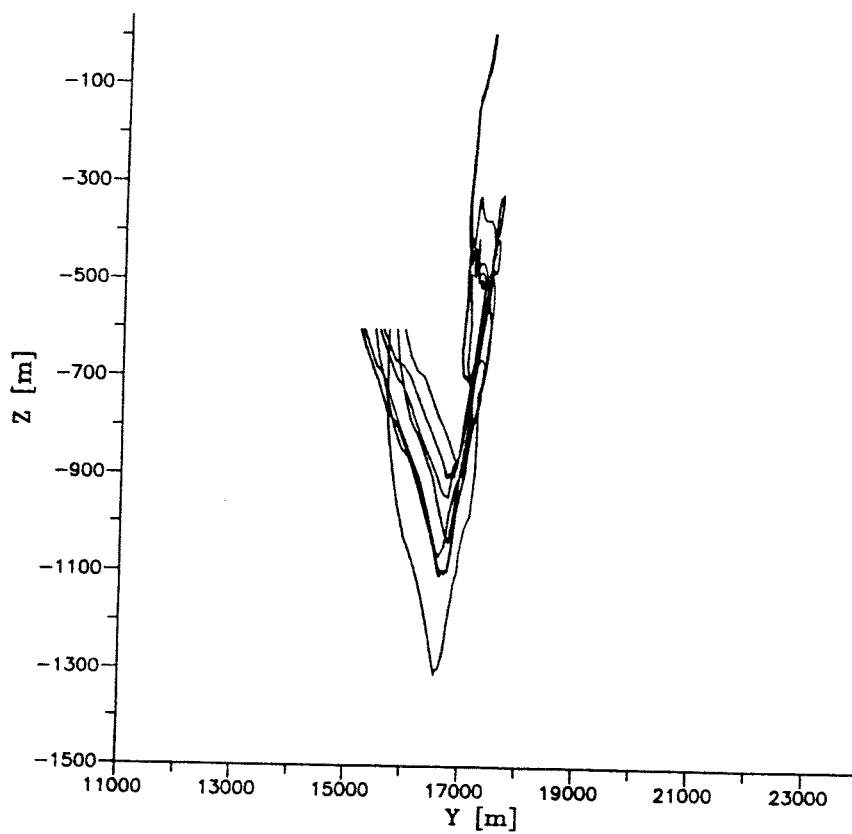


Figure B26 Vertical projection (yz-plane) of pathlines for Case X36IM.

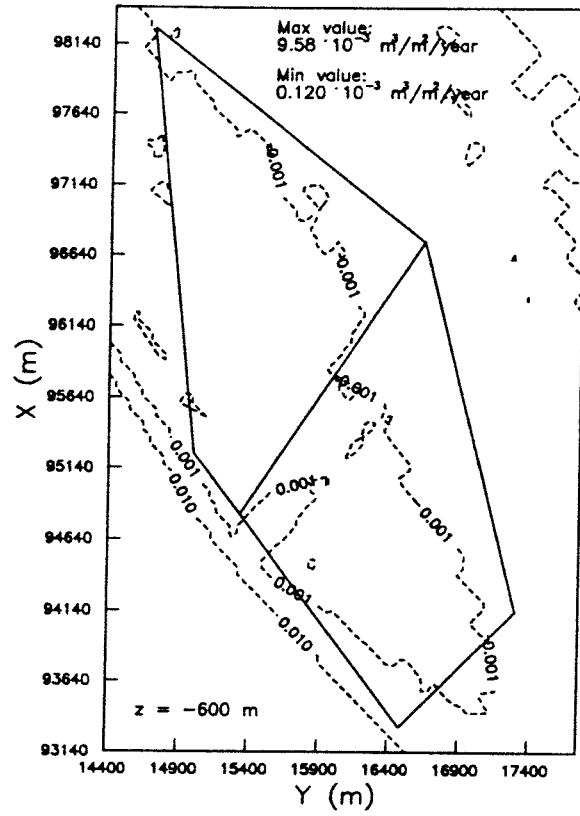


Figure B27 Contoured flux distribution ($\text{m}^3/\text{m}^2/\text{year}$) for Case X36IM.

List of SKB reports

Annual Reports

1977-78

TR 121

KBS Technical Reports 1 – 120

Summaries

Stockholm, May 1979

1979

TR 79-28

The KBS Annual Report 1979

KBS Technical Reports 79-01 – 79-27

Summaries

Stockholm, March 1980

1980

TR 80-26

The KBS Annual Report 1980

KBS Technical Reports 80-01 – 80-25

Summaries

Stockholm, March 1981

1981

TR 81-17

The KBS Annual Report 1981

KBS Technical Reports 81-01 – 81-16

Summaries

Stockholm, April 1982

1982

TR 82-28

The KBS Annual Report 1982

KBS Technical Reports 82-01 – 82-27

Summaries

Stockholm, July 1983

1983

TR 83-77

The KBS Annual Report 1983

KBS Technical Reports 83-01 – 83-76

Summaries

Stockholm, June 1984

1984

TR 85-01

Annual Research and Development Report 1984

Including Summaries of Technical Reports Issued during 1984. (Technical Reports 84-01 – 84-19)

Stockholm, June 1985

1985

TR 85-20

Annual Research and Development Report 1985

Including Summaries of Technical Reports Issued during 1985. (Technical Reports 85-01 – 85-19)

Stockholm, May 1986

1986

TR 86-31

SKB Annual Report 1986

Including Summaries of Technical Reports Issued during 1986

Stockholm, May 1987

1987

TR 87-33

SKB Annual Report 1987

Including Summaries of Technical Reports Issued during 1987

Stockholm, May 1988

1988

TR 88-32

SKB Annual Report 1988

Including Summaries of Technical Reports Issued during 1988

Stockholm, May 1989

1989

TR 89-40

SKB Annual Report 1989

Including Summaries of Technical Reports Issued during 1989

Stockholm, May 1990

1990

TR 90-46

SKB Annual Report 1990

Including Summaries of Technical Reports Issued during 1990

Stockholm, May 1991

1991

TR 91-64

SKB Annual Report 1991

Including Summaries of Technical Reports Issued during 1991

Stockholm, April 1992

Technical Reports

List of SKB Technical Reports 1992

TR 92-01

GEOTAB. Overview

Ebbe Eriksson¹, Bertil Johansson², Margareta Gerlach³, Stefan Magnusson², Ann-Chatrin Nilsson⁴, Stefan Sehlstedt³, Tomas Stark¹

¹SGAB, ²ERGODATA AB, ³MRM Konsult AB

⁴KTH

January 1992

TR 92-02

**Sternö study site. Scope of activities and
main results**

Kaj Ahlbom¹, Jan-Erik Andersson², Rune
Nordqvist², Christer Ljunggren³, Sven Tirén²,
Clifford Voss⁴

¹Conterra AB, ²Geosigma AB, ³Renco AB,

⁴U.S. Geological Survey

January 1992